Lawrence Berkeley National Laboratory

Title

Quantitative and qualitative bone imaging: A review of synchrotron radiation microtomography analysis in bone research

Permalink

Authors

Obata, Yoshihiro
Bale, Hrishikesh A
Barnard, Harold S
et al.

Publication Date

DOI

Peer reviewed

Quantitative and qualitative bone imaging : A review of synchrotron radiation

microtomography analysis in bone research

Yoshihiro Obata[a], Hrishikesh A. Bale[b], Harold S. Barnard[c], Dula Y. Parkinson[c], Tamara N. Alliston[d], Claire Acevedo[a,1,*]

[a]*Department of Mechanical Engineering, University of Utah, Salt Lake City, UT, 84112, USA*
[b]*Carl Zeiss X-Ray Microscopy, Pleasanton, CA, 94588, USA*
[c]*Advanced Light Source, Lawrence Berkeley Laboratory, Berkeley, CA, 94720, USA*
[d]*Department of Orthopedic Surgery, University of California, San Francisco, CA, 94143, USA*

Abstract

All levels of the unique, hierarchical structure of bone consisting of collagen and hydroxyapatite crystals at the nanoscale to osteon/lamellae structures at the microscale contribute to its characteristic toughness and material properties. Elements of bone's density and size contribute to bone quantity (or bone mass), whereas elements of bone's material composition, material properties, internal structure, and organization describe the quality of bone. Bone quantity and quality can be degraded by factors such as aging, disease, treatments, and irradiation, compromising its ability to resist fracture and sustain loading. Accessing the morphology and architecture of bone at the microscale to quantify microstructural features such as osteocyte lacunae and canals as well as assessing the degree of mineralization and path of crack propagation in bone provides crucial information on how these factors are influencing bone quantity and quality. Synchrotron radiation micro-computed tomography (SRμCT) was first used to assess bone structure at the end of the 1990's. One of the main advantages of the technique is that it enables accurate three-dimensional (3D), non-destructive quantification of structure while traditional histomorphometry on histological sections is inherantly deestructive to the sample and two-dimensional (2D). Additionally, SRμCT uses monochromatic, high-flux X-ray beams with high-resolution optics to provide high resolution and high contrast of bone samples. This allows the quantification of small microstructural features (e.g. osteocyte lacunae, canals, trabeculae, microcracks) and direct grayvalue compositional mapping (e.g. mineral quantification, cement lines) with greater speed and fidelity than lab-based micro-computed tomography. In this article, we review how SRμCT has been applied to bone research to elucidate the mechanisms by which bone aging, disease, and other factors affect bone fragility and resistance to fracture.

Keywords: bone, x-ray imaging, synchrotron microtomography, bone quality, bone fragility, toughness

1. Introduction

Biological materials often exhibit exceptional mechanical properties and intricate designs (Fratzl and Weinkamer, 2007). These designs are often organized hierarchically, where all structural levels contribute to the material properties at different length scales (Rho et al., 1998; Currey, 2005). Due to their unique properties, biological materials have inspired investigation from engineers and scientists, and bone is no exception (Fratzl, 2007; Wegst et al., 2015). The mechanical properties of bone are derived from its hierar-chical, multi-scale arrangement of collagen molecules and hydroxyapatite crystals at nano- to macroscopic dimensions (Rho et al., 1998; Zhang et al., 2003). At the microscopic level, mineralized collagen molecules and fibrils are organized in fiber patterns comprising the lamellar structure of the osteons in human cortical bone and the trabecular network in cancellous bone (Weiner et al., 1999). Osteons in cortical bone are cylindrical features 200 to 300 μm in diameter containing a central longitudinal cavity called the Harvesian canal (Figure 1) (Zimmermann et al., 2016; Acevedo et al., 2015; Aizenberg et al., 2005). Trabeculae in

---

*Corresponding author
[1]E-mail address: claire.acevedo@utah.edu (Claire Acevedo)

cancellous bone comprise a three-dimensional (3D) porous network of processes with a 100 to 400 μm thickness (Oftadeh et al., 2015). Features at all length scales in this complex, natural material account for bone's stiffness, strength, and toughness originate at most length-scales in this complex natural material (Launey et al., 2010a).

In addition, bone is dynamic, constantly adapting to local needs and mechanical loading through remodeling (Nomura and Takano-Yamamoto, 2000; Huiskes et al., 2000). The remodeling cycle is a homeostatic process involving bone resorbing cells (osteoclast and osteocyte cells) and bone forming cells (osteoblast and osteocyte cells) (Yee et al., 2019; Milovanovic et al., 2013a). Because bone is continuously resorbed and reformed, bone quantity and quality are, by nature, dynamic. Bone quantity, also called bone mass or bone mineral density (BMD), is the amount of mineralized bone material in a given bone volume. Bone quantity relates to the degree of bone porosity, more specifically to the density and size of these porosi-ties. Bone quality is used to describe bone material composition and material properties as well as bone microstructure and geometry, which affect whole bone's mechanical properties, such as strength and fracture resistance (Launey et al., 2010b; Schmidt et al., 2019). Although loss of bone resistance is often associated with low bone mass (Genant et al., 1999), over half of all non-vertebral fractures in people over 55 years of age occurred in those with a clinically normal bone mass (Schuit et al., 2004). Therefore, bone fragility is thought to result as well, from alterations in bone quality (Burr, 2004). Bone quality is known to be influenced by bone micro-architecture, mineral distribution linearly related to elastic properties, remodeling, and damage (Larrue et al., 2011; Seeman, 2008).
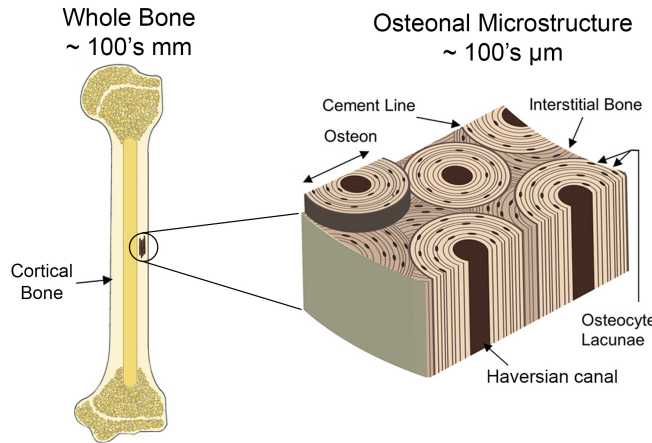

Figure 1: **Hierarchical structure of bone at the microscale.** At the macroscale, human long bone consists of trabecular (cancellous) and cortical bone. Secondary osteons (Haversian systems) in cortical bone are basic structural units at the microscale. Central to each osteon is a Haversian canal. These vascular porosities are connected to osteocytes in the Haversian system by canaliculi. Canaliculi are only observable at the nanoscale. Every osteocyte lies within small porosities called lacunae. At the boundary of each osteon is a highly mineralized cement line. (Figure adapted from Zimmermann et al. (2012); Milovanovic et al. (2013b); Acevedo et al. (2018b))

Bone quality can be compromised by age, bone fragility diseases (e.g. diabetes, osteogenesis imperfecta, and osteoporosis) or by treatments such as glucocorticoids, radiation or long-term bisphosphonate use (Felsenberg and Boonen, 2005; Acevedo et al., 2018b; Grafe et al., 2014; O'Brien et al., 2004; Zimmermann et al., 2019; Barth et al., 2010). Although these diseases and aging are known contributors to poor bone quality, the underlying mechanisms controlling bone quality were not understood at the beginning of the 21st century, making the factors that regulate bone quality extensive topics of interest in the last twenty years (Zimmermann et al., 2015a; Acevedo et al., 2018a; Alliston, 2014). Synchrotron radiation micro-computed tomography (SRμCT) techniques have provided major insight into volumetric bone structure and porosity, compositional mineral analysis, and crack path in bone fragility diseases. The first synchrotron imaging study dedicated to trabecular bone was published in 1999 (Salomé et al., 1999). This study took advantage of the high resolution and high signal-to-noise ratio imaging provided by the monochromaticity and high photon flux of of an x-ray synchrotron beam to image trabeculae. SRμCT enables major advancements in the bone research field compared to other available techniques. Traditional techniques to characterize bone structure include histomorphometry based on histological sections and lab-based micro-computed tomography (μCT) (Müller

et al., 1998). Histomorphometry on 2D histological sections only provides 2D structural information of a specific cross-sectional area. Lab-based μCT systems are widely used because of their accessibility. They have improved their efficiency and spatial resolution drastically over the last decades. However, their spatial resolution and the use of polychromatic energy above 30 keV limits their ability to image small microstructural features (e.g. osteocyte lacunae, canals, microcracks) and to perform direct grayvalue compositional mapping for mineral quantification. We are going to discuss three major advancements in understanding bone's resistance to fracture enabled by SRμCT: namely quantification of 1) porosity and structure, 2) volumetric mineral distribution , and 3) crack deflection/twisting.

Porosity and structure. SRμCT is a powerful tool for making non-destructive observations of three-dimensional features at the micrometer length-scale (Salomé et al., 1999). Size and density of porosities such as Haversian canals and osteocyte lacunae, as well as their organization in space (microstructure) are factors influencing both bone quantity and bone quality. Therefore, SRμCT became a suitable tool for assessing bone quantity and quality (Gauthier et al., 2019; Withers, 2015; Donnelly, 2011). This method consists of taking transmission radiographs at multiple angles around an object and using them to reconstruct the inner microstructure of the object computationally (Hounsfield, 1973; Kak et al., 2002b). Inspection of bone matrix porosities and microstructure can reveal changes in their size and organization that will directly impact bone's ability to sustain loading and resist fracture.

Bone quality is also impacted by its ability to remodel at the cellular level (Alliston, 2014). Specific bone cells, called osteocytes, are embedded in bone matrix and have been revealed to play an integral role in bone remodeling (Bellido, 2014). Osteocytes orchestrate the actions of osteoclast and osteoblast cells and are responsible for perilacunar/pericanalicular remodeling (PLR) and mechanotransduction (Bonewald, 2011, 2007; Dole et al., 2017). SRμCT allows for quantification of osteocyte lacunae (i.e. the small space containing the osteocyte) size, density, and distribution to reveal osteocyte remodeling activity and how they interact with the bone matrix to change bone microstructure. The study of bone fragility disease and treatments elucidates the normal mechanisms by which bone cells act to maintain biological and mechanical homeostasis in bone tissues (Dole et al., 2017; Acevedo et al., 2015). Indeed, because bone quality is a multiple length-scale dependent parameter that is heavily impacted by bone remodeling, analyzing these changes in microscale level features is an important strategy to better understand these intricate biological mechanisms and how their disruption compromises bone health.

Volumetric mineral distribution. If bone turnover performed by osteoclasts and osteoblasts is suppressed, excess mineralization of the bone matrix may occur. Regions of excess mineralization may act as a primary location for microcracking, resulting in fragile bone and ultimately impairing resistance to fracture that impedes crack growth (also called extrinsic mechanisms, see below) (Ettinger et al., 2013). Direct compositional measurement, such as mineral quantification, is one of the major advantages that SRμCT offers over lab-based μCT systems. The use of monochromatic (parallel beam) energy enables direct correlation between grayvalues and mineral attenuation. Change in volumetric tissue mineral density is useful to identify weak highly mineralized regions which are going to drive the crack extension.

Crack deflection/twisting. Bone fragility is associated with a major deterioration of bone toughness, or resistance to fracture (Inzana et al., 2013). Bone toughness results from the mutual competition of intrinsic mechanisms acting ahead of the crack tip, primarily at the nanoscale, and extrinsic mechanisms acting behind the crack tip at the microscale (Launey and Ritchie, 2009; Zimmermann and Ritchie, 2015). Extrinsic mechanisms can be visualized via SRμCT experiments. Extrinsic toughening mechanisms act to impede crack growth by crack-tip shielding. These mechanisms include crack deflection/twisting and crack bridging (Peterlik et al., 2006; Ager et al., 2006; Nalla et al., 2005a; Ritchie et al., 2006). The concepts of extrinsic and intrinsic toughening mechanisms in bone and other materials has been pioneered by the Ritchie group at the University of California, Berkeley and Lawrence Berkeley National Laboratory.

Identifying changes in extrinsic (crack-tip shielding) toughness in bone necessitates the study of bone's microstructural features. Crack deflection and twisting in human cortical bone primarily occur at the cement line located at the interfaces of osteons (Yeni and Norman, 2000). The cement line is a highly mineralized region surrounding the secondary osteons in human bone (Nobakhti et al., 2014). Growing microcracks reaching these regions will be deflected and twisted to follow the path of least resistance offered by the cement lines (Zimmermann et al., 2009). Imaging both crack deflection/twisting and its position relative to cement lines has been made available with SRμCT capabilities. In murine bone, there are no osteons or Haversian canals, instead circumferential lamellae predominate (Saban et al., 1996). These lamellae layers in murine

bone can act as delamination interfaces resulting in similar crack deflection and twisting (Carriero e t al., 2014). This results in a tortuous crack path if a crack is propagating in the transverse (breaking) direction, enhancing toughness in the transverse orientation in bone (Koester et al., 2011; Nalla et al., 2005b). SRμCT visualization of three-dimensional crack profiles and their interaction with microstructural features is helpful in studying the origins of fracture resistance (Koester et al., 2008). Toughening mechanisms also exist in the longitudinal direction of bone via crack bridging, or uncracked-ligament bridging (Nalla et al., 2004). This mechanism results in the creation of uncracked regions parallel to the crack path which carry the load that would otherwise contribute to further crack propagation (Zimmermann et al., 2012; Nalla et al., 2003). While this mechanism results in increased toughness in bone, crack bridging is not as influential as crack deflection and twist (Nalla et al., 2005b).

Here we review the current body of research on the applications of SRμCT in providing quantitative and qualitative results to assess the mechanisms that control bone quality in bone fragility disease. Additionally, we will explain SRμCT techniques and include a discussion on data acquisition and processing. Because of the advancements in computed tomography technology, the sophistication and capabilities of lab-based methods has increased in recent years. To address this, a comparison of different computed tomography methods is also performed. SRμCT data has shown how healthy bone derives its unique fracture resistance and how it can be impaired by fragility diseases or treatment. Only SRμCT can provide the three dimensional quantitative analysis of mineral density and the resolution to observe local changes in microstructure, bone matrix mineralization, and crack propagation. Finally, results from SRμCT research between different studies analyzing bone disease, bone remodeling, and treatments will be compared.

2. Synchrotron Microtomography Image Acquisition

Computed tomography (CT) is a 3D imaging process where many 2D x-ray images of a sample are acquired over a range of angles either over 180 or a complete 360 degree rotation, depending on the sample. These images are then used to computationally reconstruct a 3D image of the sample (Kak et al., 2002b; Bernhardt et al., 2004; Cano et al., 2008). CT imaging has broad applications in many fields that require the non-destructive study of complex structures such as biological, medical, and materials sciences. CT scanners typically use conventional bremsstrahlung x-ray sources that generate X-rays by colliding a low energy (energy < 500 keV) electron beams into metallic targets. These sources are very compact (10s of centimeters in length) and are bright enough to be used in a variety of applications.

For CT with micro-scale resolution, μCT, much brighter, higher flux x-ray beams are required. Because of the limits of x-ray source technology, lab-based conventional μCT scanners require many hours per scan (du Plessis et al., 2016). For brighter beams and faster scans, SRμCT is highly advantageous. Synchrotron radiation sources typically use large, circular electron accelerators (50-500m diameter) with high energy electron beams (energy: 1-10 GeV) (Barnard et al., 2017). Rather than colliding these electrons with targets, simply deflecting these beams by a few degrees with magnets causes synchrotron x-rays to be emitted. These X-rays beams are highly collimated, broad spectrum (spanning wide range of energy/wavelength), and are brighter than conventional x-ray sources by several orders of magnitude.

Due to the high X-ray flux, SRμCT scans are regularly performed in several minutes with sub-micron resolution (Stampanoni et al., 2006). With optimization of image acquisition settings, images can be taken at rates faster than 1 image/second. The rapid scans that are achieved with SRμCT are helpful for performing studies at reasonable timescales. Furthermore, they are necessary for studying biological samples because effects such as dehydration and temperature change over time can alter the dimensions of the sample, thus disturbing the CT scan process.

Depending on the source X-ray beam condition (i.e.,either parallel beam or divergent cone beam geometry), the ultimate resolution achieved can depend on several factors. In the case of parallel beam geometry typically used at many synchrotron light sources, the resolution is primarily dependent on the combination of scintillator properties, optical lens system, and detector (Carlton et al., 2016). In parallel beam geometry, the highest achievable resolution is typically limited by the wavelength of light produced in the scintillator and the visible light optics used for detection. When using a cone beam geometry, the resolution is dependent on the geometrical position of the detector from the source and sample, the source size and the camera pixel size (Langer et al., 2012b). Sometimes, cone beam geometries may combine scintillator coupled objectives

for optical magnification such as in the laboratory X-ray microscopes (Feser et al., 2008). With cone beam, the highest achievable resolution is limited by the transverse size of the X-ray source.

The size of the field of view (FOV) that can be imaged is also an important consideration. For a given camera size, there is an inverse relationship between magnification and FOV. The other limitation on FOV is the X-ray beam size (typically several cm in width and several mm in height with the exact dimensions depending on the design of the X-ray beamline and synchrotron facility). For example, a typical SRμCT instrument with a 10$\times$ objective and 0.6 micron resolution could image a 2×2 mm^2 area FOV, corresponding to 2 mm(height) $\times$ 2 mm(diameter) cylindrical volume. The same system with a lower magnification 2X objective with 3 micron resolution would be able to image a 10×10 mm^2 FOV, corresponding to 10 mm(height) $\times$10 mm(diameter) cylindrical volume. However, if the beam is only 5 mm tall this would limit the FOV in the latter case. For special cases where it is necessary to capture large samples or multi-scale structural features while maintaining high resolution, it is possible to increase the FOV with some additional complexity in the scan process. The height of the FOV can effectively be extended by taking multiple scans at different heights and stitching them together computationally. The width of the FOV can also be extended in the direction perpendicular to the axis of rotation by offsetting the axis of rotation and scanning over 360 degrees, also called wide field view tomography (Labriet et al., 2018).
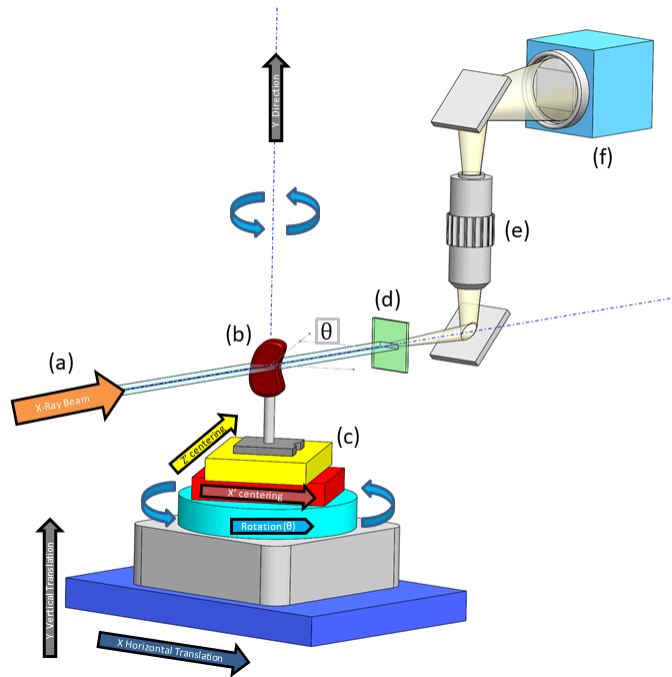

Figure 2: **SRμCT scan geometry** The X-ray beam (a) originating from the synchrotron source passes through the sample (b), creating a transmission image on the scinitallator (d). The scintillator is crystaline material that converts the X-ray image into visible light which is then imaged directly with a conventional microscope objective (e) and a digital camera (f). The sample is mounted on top of precision stage (c), which used for positioning and alignment of the sample with respect to the beam and optics. The sample can then rotated and imaged over 180 or 360 degrees.

Synchrotron hard X-ray tomography beamlines provide a number of options for adjusting settings to optimize data collection for different applications. We will discuss three of these: Monochromatic/Polychromatic X-ray energy, absorption or propagation-based phase contrast modes, and other scan parameters.

Monochromatic/Polychromatic X-ray energy. Synchrotrons produce very bright, broad spectrum X-rays, spanning a wide range of X-ray energy/wavelength. Many beamlines have an optical device called a monochromator that removes all but a narrow range of energy by preferentially reflecting X-rays of a specific energy/wavelength using a silicon crystal or multilayer mirror (somewhat similar to a diffraction grating in a spectrometer). The selected energy is dependent on the angle of the mirror and therefore the energy can be tuned for optimized contrast by tilting the mirror. Beamlines can switch between a polychromatic

"white" or "pink" beam mode and a monochromatic mode by swapping the multilayer crystal in and out of the X-ray beam path. Most quantitative studies of bone using synchrotron sources rely on monochromatic radiation because the beam energy can be tuned to an energy that maximizes the absorption contrast and minimizes imaging artifacts. Moreover, the attenuation coefficients obtained from the scan data be more easily converted to quantitative values like mineral density, based on tabulated values of X-ray absorption for particular compounds at a given X-ray energy. Polychromatic scans with a synchrotron source have the advantage of higher flux and hence can be used for higher speed scanning. However, this mode is not as commonly used for bone due to additional radiation damage caused by significantly higher flux and the less optimized broad energy spectrum

Absorption or propagation-based phase contrast modes. The most straightforward mechanism for X-ray imaging is absorption contrast. The density of a material and absorption properties of its constituent atoms are directly related to how many X-rays pass through the material to create an image. This is very effective for samples containing materials that have absorption properties that differ enough for them to be distinguished but are also close enough in absorption for either of the materials can observed within the dynamic range of the detector. In the case of bone imaging, bone inherently has a good absorption contrast and is well suited for absorption contrast tomography. Moreover, a significant part of bone research studies involve measurement of changes in mineralization as a result of a drug or due to disease.

Synchrotron beamlines can also use multiple modes of phase contrast, including grating-based, speckle-based, and propagation-based. Propagation-based phase contrast is the simplest because it requires no additional hardware or different scanning routines (Paganin et al., 2002; De Witte et al., 2009). Phase contrast in this context occurs due to small variations in the refractive index of materials in the sample. Abrupt changes in refractive properties between structures in the sample causes the X-ray paths to be slightly deflected at material interfaces, producing fringes that tend to enhance edges. Grating-based phase contrast involves using two gratings: a phase grating to introduce a phase shift which through the Talbot effect creates intensity variations and a second grating to analyze the created pattern (Talbot, 1836; Momose et al., 2003). This type of phase contrast has been used in both lab-based settings and at synchrotron sources (Ruiz-Yaniz et al., 2016). Speckle-based phase contrast methods use a speckled surface, such as sandpaper or a biological membrane, with propagation-based methods to extract differential contrast in a scan; revealing information about the phase gradient (Morgan et al., 2012; Cerbino et al., 2008). Although the first uses of this technique were performed at synchrotron facilities, the technique has been expanded to lab-based CT setups as well (Zhou et al., 2015).

Phase contrast is particularly useful for imaging when materials have low absorption and cannot be easily distinguished from each other because of their similar absorption properties. The relative contribution of phase contrast to the image can be increased simply by moving the detector farther from the sample; with increasing distance of the detector, the phase fringe arising from transitions between regions with differing indices of refraction are better resolved and hence the boundaries separating the two regions are easily discerned. Due to the high coherence of synchrotron beams, samples that have lower absorption contrast and are low absorbing produce excellent phase contrast. Because contrast is greatly dependent on the changes in the index of refraction rather than the x-ray absorption in phase contrast mode, features such as cracks, voids, and interface boundaries are clearly resolved.

Scan parameters. Scanning parameters include exposure time, the angular range of scanning and the number of projections images collected over that range, whether the scan is done in "fly scan" mode (with the sample continuously rotated during scanning), and when and how many flat field (images without the sample) and dark field (images without X-ray illumination) images are collected. The major consideration in setting these parameters is the trade-off between scan time and image quality. Faster scans can help reduce delivered radiation dose or sample motion issues (mostly associated with dehydration in bone samples), but also have lower signal to noise due to few X-rays reaching the detector for each image. The process of optimizing these scan parameters is often closely tied to the image processing—the scans are often set to be run as fast as possible, to take advantage of limited synchrotron beam availability, while still enabling the image processing goals to be accomplished.

In addition to scan parameters, additional considerations must be made to account to irradiation of bone samples during scanning. This is usually the case when bone scans are taken in absorption mode to take advantage of the direct conversion of gray values into attenuation coefficients. In particular, in situ mechanical testing can expose bone to about 1 MGy of radiation. Ritchie and his group have shown that

x-ray radiation, typically used in microtomography, degrades the mechanical properties of bone (Barth et al., 2010; Cornu et al., 2000). The total radiation dose need to be kept under 30 kGy to limit the detrimental effect of x-ray exposure (Barth et al., 2010, 2011). Decreases in ultimate strength, ductility, work-to-fracture, and fracture toughness were observed once the 30 kGy limit is reached (Barth et al., 2010). When comparing crack propagation in the transverse direction of bone using SRμCT between low radiation dose and high dose, large deflections in the crack path are present in the low dose case while much lower severity deflection and twist are present in the high dose (Barth et al., 2011) indicative of toughness decrease. To decrease radiation dose when imaging a crack path, phase contrast mode is used to increase the sensitivity and contrast of a scan, enhancing the crack for a given radiation dose (Lewis, 2004). Managing radiation dose to mitigate alteration of bone properties is an important consideration to make when performing SRμCT if mechanical testing is performed following a scan.

3. Synchrotron Microtomography Image Processing

Following acquisition of SRμCT data, tomographic slices must be reconstructed. In SRμCT, X-ray projections of a sample being scanned are collected at multiple angles between 0 and 180 degrees or between 0 and 180 (or 360) degrees of rotation (MacDowell et al., 2016). A Fourier transform is performed on the projection data to obtain location estimates of the object's Fourier transform in the frequency domain along radial lines (Smith, 2003). Ideally, the reconstruction of each projection angle could be summed to obtain information on the entire frequency domain to provide a complete, full reconstruction. However, this is not the case because each projection is only representative of a single radial line, resulting in features possessing a diffuse blur. To correct this blur, a filtered backprojection algorithm can be applied (Peters, 1997; Salomé et al., 1999). Filtered back-projection applies weighting to the frequency domain data, effectively allowing positive and negative components of the filtered projection to cancel during summing, and thereby eliminating the diffuse blur (Kak et al., 2002a). Commercial reconstruction software such as Octopus (Octopus v8; IIC UGent, Zwijnaarde) or python-based reconstruction through the TomoPy package relies on this image reconstruction method to obtain transverse slices relative to sample orientation during scanning (Gürsoy et al., 2014). Reconstructed data is processed using image processing tools, such as ImageJ (Rasband, W.S., ImageJ, US National Institutes of Health, Bethesda, http://imagej.nih.gov/ij/, 1997–2011.), Avizo (VSG, Visualization Sciences Group), and Dragonfly (ORS, Object Research Systems) to extract information about microstructure and crack propagation.

When processing SRμCT data, artifacts from the scanning process must be removed to ensure accurate material characterization (Schlüter et al., 2014). To achieve the best possible accuracy, key, undesirable artifacts must be removed during or after reconstruction (Vidal et al., 2005). Additionally, proper segmentation techniques must be performed during image processing to accurately quantify bone (Dong et al., 2014). The main scanning artifacts that are present in SRμCT data include stripe or ring artifacts, beam hardening, metal or attenuation coefficient artifacts, and shifted rotation center (Bouxsein et al., 2010). Stripes in the original, scanned data, which appear as rings in reconstructed data (Figure 3a), are a result of inhomogeneous X-ray beam drift (Gürsoy et al., 2014). Defects on the scintillator or the detector of the synchrotron system can exacerbate these effects (Raven, 1998). This defect can be an issue because grayvalues of pixels/voxels can be altered and features of the microstructure can be obscured. To remove ring artifacts, combined wavelet-Fourier filtering is often implemented on the dataset before reconstruction to remove stripes (Münch et al., 2009).

Phase contrast can be a source of artifacts if it is not taken into account and images are assumed to be based purely on absorption (Vidal et al., 2005). In the context of SRμCT, the type of phase-contrast that is contained in iamges is reffered to as "propagation-based" phase contrast, and is a result of the scanned sample distorting the X-ray wavefront, causing edges and internal features of the bone to be highlighted with much higher or much lower intensity pixels than what is truly present (Figure 3c) (Mayo et al., 2012). Not accounting for phase contrast contributions to images will lead to error when quantifying mineralization, also called volumetric tissue mineral density (vTMD), because pixel grayvalues are assumed to be directly related to levels of mineralization. The influence of phase contrast can interfere with detection of mineral heterogeneities that may be present at boundaries near pores in bone.

Phase-retrieval techniques can be used to quantitatively reconstruct pixel grayvalues corresponding to the phase contrast. One popular approach to phase retrieval works by solving the 'Transport of Intensity

Equation' (TIE) (Paganin et al., 2002). However, phase retrieval generally degrades image resolution, and is only quantitatively valid under assumptions that are often not met in bone samples (for example, that the sample is made of only one type of material).

While phase contrast can be problematic when studying vTMD, it can be beneficial - and in fact critical -in other bone and biological materials research. For instance, detecting microcracks and mapping out fracture in mechanically loaded bone samples, from either in situ or ex situ experiments is highly challenging especially when the cracks have not opened up sufficiently greater than the scan resolution (Larrue et al., 2011; Thurner et al., 2006). In such situations, the phase contrast mode is used. Phase-contrast signal from cracks arises quite strongly and highlights the cracks much more effectively (Sinnett-Jones et al., 2005). Segmenting the crack network is however not trivial, where conventional thresholding methods or edge detection algorithms fail and requires manual to semi-automated or machine learning/deep learning segmentation (Liu et al., 2019; Zou et al., 2019; Wu et al., 2019).

Implanted objects, commonly metal, often have much higher linear attenuation coefficients (Akça and Erzeneoğlu, 2014). In a scan, these objects may cause total absorption of the X-ray, resulting in bright objects with star shaped reconstruction artifacts (Bouxsein et al., 2010). While metal artifacts in scans are greatly reduced with the use of synchrotron radiation, elimination of these artifacts can only presently be performed by removal of the object from the scan (Le Cann et al., 2019). Finally, detection of the proper center of rotation is necessary for a high-quality reconstructed dataset. Improper detection of a center of rotation results in obscured microstructural features during reconstruction (Figure 3b). Center of rotation optimization is commonly performed to detect and minimize these effects (Cheng et al., 2018).
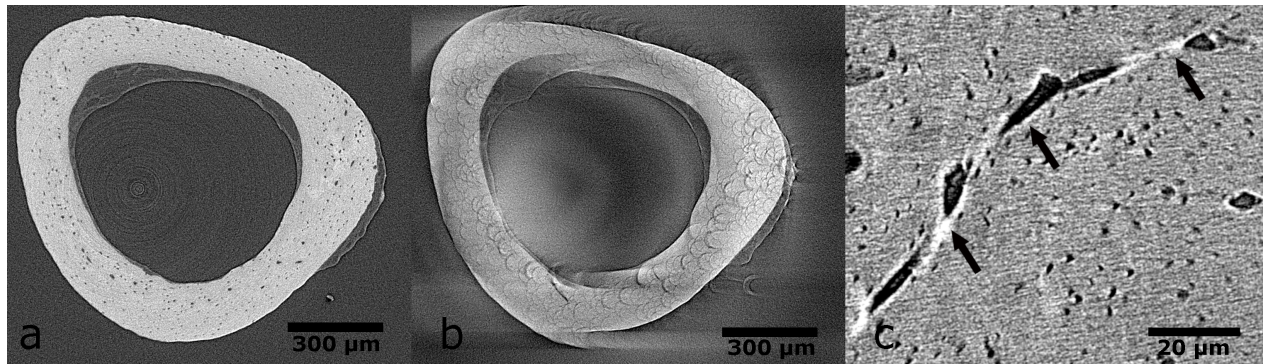

Figure 3: **Common artifacts present in SRμCT scans.** (a) Murine cortical bone cross-section. A ring artifact manifests itself as concentric circles about the rotation center in a scan. Often times these are the result of defects on the scintillator during scanning. (b) Murine cortical bone cross-section. Improper detection of the center of rotation during the image reconstruction process can result in undesirable center-of-rotation-shift artifacts , causing porosities and other microstructural features of bone to appear as crescent-shaped blurs. (c) Bovine cortical bone cross section. While still high resolution and relatively high quality, phase-constrast artifacts, indicated by black arrows, are present in the form of higher and lower intensity pixels around an edge or porosity in bone.

After producing a high-quality reconstructed dataset devoid of artifacts, proper segmentation techniques must be applied to obtain characteristic results. In analysis of trabecular bone, the volume of interest can be selected by hand or can be separated from the bone using algorithms (Buie et al., 2007). In the quantification of SRμCT data for cortical bone, segmentation is commonly performed to extract lacunar volume, canal diameter, orientation of microstructural features, examine crack propagation, or to find a host of other variables. Failure to accurately segment these features will result in a poor quantification on all successive analyses (Dong et al., 2014; Núñez et al., 2017; Carter et al., 2013). Various methods are used to segment lacunae and canals, but a large majority involve thresholding voxels within a certain range of grayvalue intensities and filtering a region based on appropriate particle size (Dong et al., 2014; Jameson et al., 2013; Jáuregui et al., 2016). Segmentation of cracks can be more challenging than osteocyte lacunae and vascular canals, but has been performed in several studies (Busse et al., 2013; Zimmermann et al., 2012; Acevedo et al., 2015; Zimmermann et al., 2015b). Segmentation of microcracks in bone using SRμCT can prove even more difficult, as noise and artifacts from the scan obscure these features (Ma et al., 2016; Larrue et al., 2007). Despite this, some successful efforts have been made (Larrue et al., 2011).

4. SRμCT and Computed Tomography in Bone Research

4.1. Computed Tomography Quantification Parameters

While SRμCT is a powerful method for investigating a variety of bone quantity and quality related parameters, it is not always the most appropriate computed tomography method. Depending on the parameters that are desired for a given study, different techniques, whether SRμCT, lab-based μCT, or synchrotron radiation nano-computed tomography (SRnCT), can be used to accomplish the task.

The technique chosen is often determined by the spatial resolution necessary to resolve key features. Choosing a technique which does not possess a high enough spatial resolution for a task will result in an inability to quantify parameters of interest. However, other factors will also influence the choice of the technique such as energy and flux range mostly suited to obtain high-contrast images and high signal-to-noise ratio in the material, or monochromaticity versus polychromaticity (for more details see Table 2). Outlined in Table 1 are selected, common bone parameters quantified by computed tomography methods.

	Parameter	Description	Modality
Bone Quantity and Size Parameters	Tb.N	Trabecular Number	LabμCT, SRμCT
	Tb.Th	Trabecular Thickness	LabμCT, SRμCT
	BV/TV	Bone Volume Fraction	LabμCT, SRμCT
	Ct.Th	Cortical Thickness	LabμCT, SRμCT
	Ct.Ar	Cortical Area	LabμCT, SRμCT
	Ca.Dm	Canal Diameter Canal	SRμCT, SRnCT
	Ca.Dn	Density Cortical	SRμCT
	Ct.Po	Porosity Lacunar	SRμCT
	Lc.V	Volume Lacunar	SRμCT, SRnCT
	Lc.S	Surface Area Lacunar	SRμCT, SRnCT
	Lc.Dn	Density Canalicular	SRμCT , SRnCT
	Can.Dm*	Diameter Canalicular	SRnCT
	Can.N*	Number	SRnCT
Bone Quality Parameters	Tb.Sp	Trabecular Separation	LabμCT, SRμCT
	Ca.Sp	Trabecular Separation	LabμCT, SRμCT
	TMD	Tissue Mineral Density	LabμCT (indirect), SRμCT, SRnCT
	SMI	Structural Model Index	LabμCT, SRμCT
	DA	Degree of Anisotropy	SRμCT, SRnCT
	Ca.Conn*	Canal Connectivity	SRμCT, SRnCT
	Can.Conn*	Canalicular Connectivity	SRnCT

Table 1: **Common Micro-Computed Tomography Parameters.**
* Canalicular variables are sometimes referred to with the abbreviation "Ca.", however, this work will use "Can." to distinguish this variable from canals.

Bone quantity is assessed through parameters related to porosities size (Th, Dm, S, Ar, V) and density (Dn, N) since they evaluate the amount of bone volume fraction (BV/TV, Po). Bone quality's parameters involved structure and organization of material in space (Sp, SMI, DA), material composition (TMD), and osteocyte-mediated remodeling (Lc, Can) .

TMD, or mineralization, is often reported as a mass of hydroxyapitite per volume or as a calcium percentage. The gray value, or voxel attenuation, of a reconstructed SRμCT scan, can be directly converted to vTMD values using the linear attenuation coefficient of the material being scanned (Nuzzo et al., 2002). This coefficient is dependent on the x-ray energy, material, and material thickness used during scanning (Burghardt et al., 2007). Finite element models can be constructed from each SRμCT scan. vTMD values of each voxel can then be assigned to a voxel-specific Young's modulus for each finite element using a power-law relationship (Wagner et al., 2011; Nyman et al., 2015; Easley et al., 2010; Wang et al., 2015).

Another advantage of high-quality images obtained by SRμCT is the possibility to calculate reliable and precise measure of strain based on Digital Volume Correlation (DVC) (Gillard et al., 2014; Palanca et al., 2016). DVC can be applied to any 3D images of a material from a reference to deformed states in order to calculate the full 3D displacement and 3D strain maps. However, when strains obtained from SRμCT are

compared with the ones obtained from LabμCT, the error is reduced by one order of magnitude, and can therefore be used to evaluate strain in the physiological range (Palanca et al., 2017; Dall'Ara et al., 2014).

Canalicular diameter (Can.Dm), number (Can.N), and connectivity (Can.Conn) are parameters that have been quantified using nanotomography techniques in recent years. Due to the existence of canaliculi at the nanoscale in bone, extremely high resolutions are needed to visualize and quantify these structures. At this length scale, bone is studied at the cellular level using SRnCT, often with phase contrast (Peyrin et al., 2014a). SRnCT, with atypical resolution of 30 to 100 nm, is a powerful technique allowing for 3D visualization of bone ultrastructure (Langer et al., 2012b; Hesse et al., 2015b; Peyrin, 2009; Peyrin et al., 2014b), including canaliculi which were not previously visible with other forms of tomography (Langer et al., 2012a). However, the FOV, and thus the sample size, are reduced. For instance, a SRnCT scan with an image resolution of 50 nm implies aproximately a $0.15{\times}0.15$ mm^2 area FOV, corresponding to 0.15 mm(height) $\times$ 0.15 mm(diameter) cylindrical volume. Quantification of the branching properties and number of canaliculi in relation to lacunae has been performed with SRnCT in addition to 3D visualization (Varga et al., 2015; Yu et al., 2020). Because of the increased resolution, highly localized effects can be captured compared to SRμCT. One such example is the mass density directly surrounding the lacunae and canaliculi. Gradients of this distribution are more pronounced near lacunae and diminish with age (Hesse et al., 2015a). With phase SRnCT, 3D organization of the mineralized collagen fibrils oscillations was revealed confirming fibril oscillations in a twisting plywood structure around osteons (Varga et al., 2013). Although SRnCT provides higher resolution images compared to SRμCT, SRnCT possesses its own set of new challenges. While resolution is high using SRnCT, this comes at the expense of a smaller field of view when scanning the sample. SRnCT beamlines are more limited in their availability when compared to SRμCT, which are also relatively limited compared to lab-based μCT. The high resolutions of SRnCT scans are limited by the detector at the beamline as well as the radiation dose. Optimization of scanning parameters allows for simultaneous radiation dose reduction and higher signal to noise ratio (Pacureanu et al., 2012).

4.2. Differences Between Lab-based μCT and SRμCT

With the increasing power of lab-based μCT, the capabilities of these systems and SRμCT begin to overlap. New lab-based systems can resolve features at similar length scales to their synchrotron counterparts (0.5 μm) via extremely small spot sizes, charged couple device cameras with smaller pixels, and high resolution scintillator-based magnification objectives. Additionally lab-based systems are more compatible for experiments spanning a long duration of time due to limited synchrotron beamtime access. On the other hand, synchrotron sources have several key advantages over conventional μCT and are user facilities which are free of cost if a beam time session is granted. Table 2 presents notable advantages and disadvantages of each method pertaining to significant factors of both techniques.

	LabμCT	SRμCT
Resolution	• Approaching approximately 0.5 μm through either detector-based or source-based system design (Zabler et al., 2020) • Lab-based systems are also achieving nanoscale resolutions of 50 nm through the use of x-ray optics, such as Fresnel zone plate optics (Feser et al., 2008)	• Resolutions ranging from 30 nm to 0.5 μm are routinely achieved at synchrotron light sources using visible light optics or x-ray optics such as zone plates and compound reflective lenses (Weitkamp et al., 2010; Stampanoni et al., 2006)

Flux	• Low flux (roughly three orders of magnitude lower than the flux in SRμCT). When lab-based systems try to push the flux though increase in power, there is an inevitable increase in spot size, leading to reduced resolution (Zabler et al., 2020).	• Synchrotron beamlines, especially ones with an associated insertion device, can deliver extremely high flux even at high resolutions (Weitkamp et al., 2010). • The abundance of flux at synchrotron sources may inadvertently lead to sensitive samples receiving higher doses of radiation. This can change material properties, especially as seen in bone (Barth et al., 2010).
Energy Range	• Typically, lab-based systems can cover a much wider range of energies than SRμCT ranging from 30 keV to up to 300 keV. However, these systems cannot access some of the lower keV ranges necessary for biological samples. Also, lab sources tend to possess a nonlinear keV to flux behavior and generally have far lower flux at lower energies, resulting in great difficulty when performing in situ experiments on biological samples in reasonable amount of time	• Users can access lower side of the energy range, typically below 10 keV. These ranges are particularly well suited for obtaining higher contrast in biological samples
Monochromaticity	• LabμCT systems typically operate based on polychromatic X-ray sources and lack tunability in scan energy	• Single crystal multilayers allow for fine tuning of the source so that monochromatic X-rays of chosen energies are available. Choosing low energies can produce significantly higher contrast in samples such as bone where the differences in mineral density are relatively small (Stampanoni et al., 2006) • Facilitates dual energy scanning approaches to take advantage of enhanced contrast at different energies from different constituents (Ito, 2005).

Artifacts	• Beam hardening artifacts are significantly present since there is higher absorption of lower energy X-rays leading to an artifact of higher intensity values on the edges of samples. • Ring artifacts on LabµCT systems are also encountered but are more easily managed, especially because the scintillator or camera response does not change much over a period of time.	• No beam hardening artifacts are observed in scans utilizing monochromatic X-rays. • Scintillators degrade faster due to higher flux. Scintillator degradation can lead to ring artifacts in the reconstructed 3D data. Secondly, most beamlines cater to a wide range of applications, requiring switching between a wide variety of experimental setups. These factors lead to a challenge in managing the scintillator optimizations that are key to ring artifact-free images
Mineral Quantification (vTMD)	• Grayscale values of reconstructed data do not directly correspond to attenuation coefficients. In order for a quantitative analysis of the mineral concentrations in bone, a calibration using known phantoms is required, involving additional steps and effort (Schweizer et al., 2007)	• One of the greatest advantages, among many others, of using synchrotron radiation for bone research. The grayscale value within a reconstructed volume directly corresponds to the attenuation coefficients of the minerals and constituents of the bone, hence the results can directly be used to correlate with other 2D mapping techniques (Bayat et al., 2005)
Scan Times	• Due to low flux, the scan times for a tomographic scan can range between 30 mins to 10s of hours depending on the chosen resolution and sample size	• Scan times typically range from a few seconds to tens of minutes depending on the mode and resolution of the measurement • High flux and advancements in sample stage and detector hardware have enables dynamic tomography with sufficiently high temporal resolution
Accessibility and cost	• LabµCT systems are widely avail-able and low cost.	• Access to synchrotron facilities is limited. Beamtime is allocated through peer-review and open competition. Users have access to free but limited beamtime of usually a few 24-hour beamtime shifts.
In situ experiments	• LabµCT systems are geared towards long-duration in situ experiments due to longer scan times and better accessibility.	• In situ experiments need to be short due to limited beamtime access. Fast scan times enables in situ quasi-static and dynamic mechanical testing of materials.

Environmental chambers	• LabμCT systems do not usually include environmental chambers (except for in situ mechanical loading).	• In situ environmental cells are usually an important part of synchrotron beamline programs. They are used to impose unique controlled environmental conditions on samples such as different levels of temperature, pressure, humidity or vacuum.

Table 2: **Comparison of lab-based μCT and synchrotron-based μCT.** Relevant advantages and disadvantages of LabμCT and SRμCT are shown for a variety of pertinent characteristics of each technique.

5. Application of SRμCT in Bone Research

Trabecular bone's mechanical behavior is strongly influenced by mircroarchitectural features whereas cortical bone's mechanical behavior is primarily dominated by the material properties (Bayraktar et al., 2004; Burr, 2002). Bone is an organized multiscale arrangement of collagen and mineral at nano- to macroscopic dimensions. As such, it derives its unique mechanical properties over multiple length scales (Reznikov et al., 2014). At micron-scales, extrinsic toughening originates from the nature of the crack path in inducing crack deflection and bridging mechanisms (Nalla et al., 2005b). SRμCT provides a unique, non-invasive means for 3D characterization of cracks and their interaction with the bone-matrix structure.

SRμCT is powerful for the analysis of biological features in bone because it provides insight into both biological mechanisms and into the control of bone quality. The ability of SRμCT to quantify thousands of lacunar volumes in 3D overcomes the limitations of more traditional histological approaches, in which analysis of lacunar size are time-consuming and based on a single 2D section through each lacunae. Quantification and visualization of the degree of mineralization, particularly around other biologically relevant features, can illuminate the mechanisms controlling matrix mineralization. Likewise, analysis of the size, tortuosity, and density of Haversian canals provides insight into bone vascularity and organization. Unfortunately, at this time, analysis of canalicular features is only possible with SRnCT. This information is incredibly valuable for understanding bone microstructure at even smaller length scales. All of these outcomes have the potential to change bone quality and toughness.

Ritchie and collaborators have used this technique to understand how various biological factors can change the bone's complex structure and thereby affect its resistance to fracture. They found that bone's ability to resist crack propagation is affected by aging (Koester et al., 2011; Zimmermann et al., 2012), long-term bisphosphonate treatment (Acevedo et al., 2015), corticosteroid treatment (Fowler et al., 2017), vitamin-D deficiency (Busse et al., 2013), irradiation (Barth et al., 2010, 2011), as well as orientation (Koester et al., 2008) and multiaxial loading (Zimmermann et al., 2009) with underlying biological and material mechanisms at the microstructural level observable with SRμCT.

In addition, collaborations with the Alliston and Acevedo laboratories have revealed the critical role of osteocytes in PLR (Dole et al., 2017; Mazur et al., 2019; Fowler et al., 2017; Dole et al., 2019). By studying mice deficient in osteocyte-mediated PLR, these laboratories found that disruption of osteocyte remodeling function can cause a distinctive pattern of hypermineralization, as well as changes in osteocyte size and distribution, both of which are associated with bone fragility.

5.1. Microstructural Features

Bone-embedded osteocytes account for 90% to 95% of bone cells (Bonewald, 2011). Osteocytes connect with one another and with the vascular network through their dendritic processes, which extend through channels called canaliculi (Bonewald, 2006). Until recently, osteocytes were widely thought to lay relatively dormant in the bone matrix where they coordinated the activity of other cell types involved in bone remodeling. Osteocytes are now known to be responsible for localized bone remodeling through PLR remodeling

as well as mechanotransduction (Qing et al., 2012; Klein-Nulend et al., 2005). During PLR, osteocytes dynamically remodel the lacuno-canalicular network through resorption and replacement of the surrounding bone matrix (Qing and Bonewald, 2009; Dole et al., 2019). Mechanotransduction is the process of converting physical cues, such as fluid flow though canalicular networks, to biochemical signals that influence cellular behaviors, which can impact bone remodeling and other factors of bone homeostasis (Burger and Klein-Nulend, 1999).

Osteocyte cells themselves cannot be easily studied with SRμCT, but SRμCT analysis of their effects on the lacunae and bone matrix can provide insight into their remodeling function and agency on bone quality (Bonewald, 2011; Nicolella et al., 2006; Gerbaix et al., 2017). Among the parameters that can be investigated using SRμCT to elucidate osteocyte function are vTMD of bone, as well as lacunar volume, density, and orientation. Porosities in bone can be segmented by size and quantified to obtain information about lacunae.

Due to the relationship between osteocytes and PLR, suppression of PLR can appear in SRμCT datasets as changes in lacunar size and orientation (Hesse et al., 2014b, 2015b; Roschger et al., 2019). The suppression of PLR through glucocorticoid-induced osteonecrosis reveals a decrease in lacunar volume in osteonecrotic bone compared to a non-treated, control bone. The significant change to both trabecular and cortical bone within 7 days of treatment extends surmounting evidence that PLR is indeed a dynamic process required for healthy bone homeostasis (Fowler et al., 2017).

Other agents that regulate cellular functions in bone also affect lacunar parameters in a variety of ways. While the precise causes of changes in osteocyte lacunar size and shape remain unanswered, it is clear that osteocytes dynamically respond to stimuli. Lacunar size is increased with a vitamin d deficiency, while lacunar density remained the same (Figure 4) (Busse et al., 2013). Long-term glucocorticoid treatment can also increase lacunar size (Lane and Yao, 2010). Lacunar size and density are additionally reported to vary with location, consistent with the anatomically distinct control of bone quality and PLR (Hesse et al., 2014a). SRμCT revealed the osteocyte requirement for the enzyme MMP13 for PLR in long bones such as the femur and tibia (Mazur et al., 2019). It also demonstrated that cochlear bone maintains lacunar parameters independently of this protein. The extent to which the differential regulation of PLR is responsible for the dramatically different material properties in long bone and the cochlea remains to be fully elucidated. Nonetheless, analysis of these microstructural features in small bones from genetically modified mice is sufficient to reveal new biological mechanisms by which cochlea bone apparently suppress osteocyte-mediated PLR to protect hearing (Jáuregui et al., 2016).

The Haversian system, or secondary osteon, is comprised of a central Haversian canal surrounded by concentric lamellae layers. The boundary of the Haversian system is marked by a highly mineralizaed cement line (Figure 1) where microcracks often form. Because Haversian canals are vascular porosities, they can be identified by SRμCT for three-dimensional visualization (Cooper et al., 2011). Efforts have also been made to visualize the canals with the surrounding osteon (Maggiano et al., 2016).

Simply visualizing Haversian canals is useful for qualitative analysis of bone quality in diseases such as Paget's disease of bone (PDB). One characteristic of this disease is hypervascularization (increased number or density of blood vessels) in bone and highly disorganized, immature lamellae surrounding disoriented Haversian canals (Zimmermann et al., 2015b). Vitamin D deficiency sees an increase in cortical porosity with a correlated increase in Haversian canal diameter (Busse et al., 2013). The effect of aging on Haversian canals has also been quantified using SRμCT. Aged bone was noted to have three times the osteonal density, indicated by comparing young and aged Haversian canal density (Figure 4) (Zimmermann et al., 2012). A higher density of Haversian canals implies an increase in the number of cement lines on osteonal boundaries. These hypermineralized cement lines have been shown to accumulate microcracks and deflect and twist the crack path.

5.2. Crack Propagation and Fracture

Healthy bone's unique ability to resist fracture is due in part to extrinsic toughness mechanisms at the microscale. However, these mechanisms can be impeded, resulting in bone fragility and an increased risk of fracture. Aging has long been known to have a detrimental effect on toughness in bone due to decreasing bone mass, or quantity, with age, but in the past two decades bone quality has emerged as an additional, potent source of bone degradation.
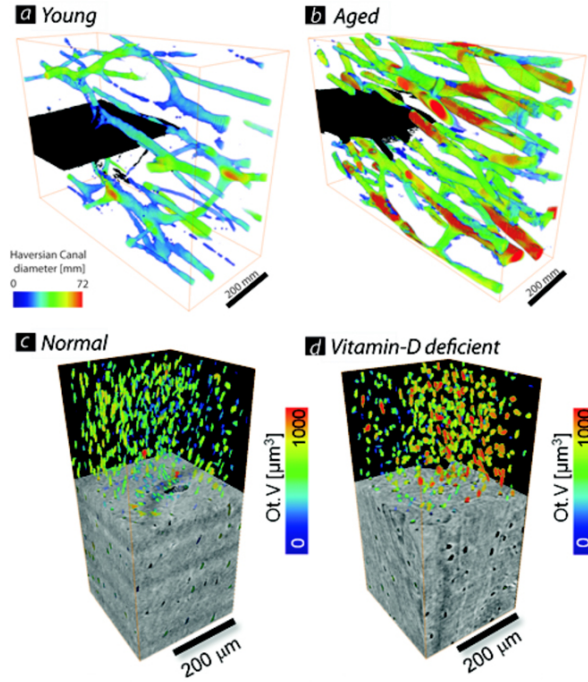
Figure 4: **Morphology changes due to aging and vitamin-D deficiency.** 3D images quantifying the size and distribution of Haversian canals in (a) young and (b) aged bone demonstrate how a higher density of canals and osteons with aging leads to a reduced toughness in the longitudinal orientation because there is more cement lines where microcracks can accumulate (Figure adapted from Zimmermann et al. (2012)). Vitamin-D deficiency alters the morphology of bone causing larger osteocyte lacunae (c and d) (Figure adapted from Busse et al. (2013)).

In the longitudinal direction of bone, presence of crack bridging is a driving mechanism of resistance to fracture. Crack bridges running parallel and forward of the crack tip act to carry load which would otherwise contribute to further propagating the crack. These bridges are observed to be smaller and less frequent in aged bone when compared to young bone (Zimmermann et al., 2012). Using SRμCT, Haversian canal density, and thus osteonal density, is shown to be notably higher for aged bone (Figure 4). The osteonal boundary possesses highly mineralized cement lines on which fracture can more easily propagate. While the osteonal boundary can possess beneficial microcracks that provide extrinsic toughening in bone, the smaller, less frequent microcracks due to aging, in combination with the increased potential surfaces for crack propagation in cement lines, result in the less tough, more brittle elderly bones. A reduction in the fracture toughness crack-resistance curve (or R-curve) slope for aged bone compared to young bone is in agreement with these mechanisms.

When a crack is propagating transversely to the osteon direction, crack deflection plays a dominant role in increasing extrinsic toughness at the microscale. While crack bridging primarily takes effect in the longitudinal direction of propagation along osteon boundaries, crack deflection acts most dominantly when cracks propagate in the transverse direction (Ritchie et al., 2009). This mechanism deflects, or changes the angle of, the direction of crack propagation from transverse to more longitudinal (Figure 5). Again, osteons are key features for this mechanism in human bone, as crack deflection commonly occurs at the osteon boundary along cement lines where a path of least microstructural resistance is found. Because osteons are oriented longitudinally, toughness in the transverse direction is markedly higher (i.e. when the maximum driving force propagates the crack in the direction perpendicular to the osteons), by approximately five times more than in the longitudinal direction (Koester et al., 2008). In lamellar murine bone, crack deflection is also shown without the presence of osteons. In this case, the crack is deflected by the lamellae acting as delamination barriers to increase toughness (Carriero et al., 2014).

Crack deflection and toughness are often adversely impacted by bone disease, and SRμCT has been used in combination with other techniques to elucidate mechanisms that affect toughness. Osteogenesis imperfecta

(OI), brittle bone disease, is an ailment in which molecular level mutations in bone are responsible for sudden whole-bone fracture (Sillence et al., 1979). A comparison of crack path deflections in whole bone fracture from OI with healthy bone has revealed that wild-type, healthy bone crack propagation in the transverse direction has marked deflections and a tortuous crack path and OI has a characteristically smoother crack path (Carriero et al., 2014). In combination with R-curve analysis, it is clear that toughening mechanisms in OI bone are highly disrupted. When comparing healthy bone and PDB, crack growth of control bone displays large crack deflection at the longitudinally-oriented osteon boundaries, where PDB shows a distinctly straighter propagation in the transverse direction due partly because of the previously mentioned disorganization of Haversian canals/osteons. Despite these features of the diseased bone, there is no significant difference in energy dissipation or crack-growth toughness between control and PDB samples. In the absence of crack deflection due to disorganization of the Haversian systems, increased plasticity of the bone and crack bridging have more pronounced effects, which partially compensate for the lack of crack deflection (Zimmermann et al., 2015b). The complexity of bone's hierarchical structure as well as the mechanisms that influence toughness in bone have profound effects on crack deflection.
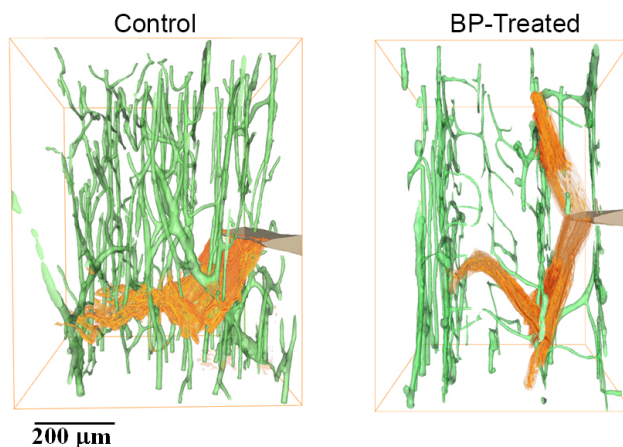

Figure 5: **Tomographic image showing the crack path from a notch oriented perpendicular to the osteonal orientation.** Both control and bisphosphonate treated shows samples show the crack path (in orange) deflecting and twisting in relation to the bone's structure (i.e., specifically at the Haversian canals, which are shown in green) (Figure adapted from Acevedo et al. Bone 2015).

5.3. Mineralization

vTMD is a component of bone quality made directly accessible using SRμCT. When analyzing SRμCT data for application in bone research, the shift in peak vTMD is studied as a measure of change in miner-alization. The extremity regions of the mineralization curve can be indications of hypo- or hypermineraliza-tion, with an increased percentage of low mineralization values (low calcium weight percentage) indicating hypomineralization and an increased percentage of elevated mineralization values indicating hypermineralization. Because an average of the vTMD can normalize these differences, examining the distribution of mineralization is important. These mineralization parameters provide valuable information on the effects of disease or genetic modifications on the bone matrix. For example, in vitamin D deficient bone, a shift towards higher peak calcium weight percentage was observed with distinct regions of hypermineralization. Findings from this study indicate that a vitamin D deficiency may be related to marcoscale loss of bone quality and increased fracture risk (Busse et al., 2013). In contrast, hypomineralization and a shift towards lower peak calcium weight percentage in PDB may partially be responsible for increased plasticity and a compensatory effect on bone fragility (Zimmermann et al., 2015b).

In some cases, hypermineralization is associated with alterations in osteocyte-mediated PLR and may be a potential contributor to bone fragility. The relationship between PLR and mineralization was investigated as part of a study evaluating glucocorticoid-induced osteonecrosis (Figure 6). These studies highlight a major advantage of SRμCT. Because of its ability to rapidly and precisely collect large amounts of quantitative data
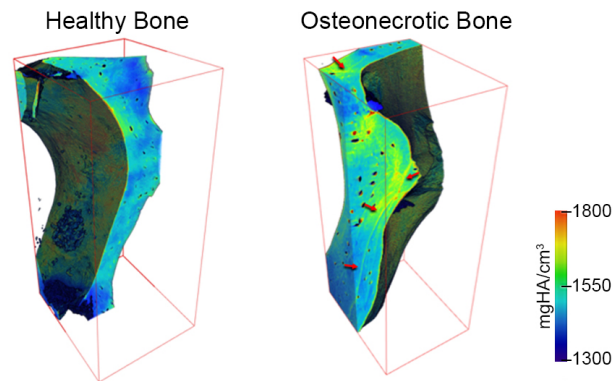
Figure 6: **Changes in mineralization due to glucocorticoid-induced osteonecrosis.** Hypermineralization of osteonecrotic bone (arrows) compared to healthy bone from the human femoral head shows the role of perilacunar remodeling. (Figure adapted from Fowler et al. Sci Rep 2017).

on mineralization and lacunar size, SRμCT offers sensitivity that is currently available in no other technique. Although histological methods could not detect a glucocorticoid-dependent repression of PLR until 21 days of treatment, SRμCT detected PLR suppression within 7 days of glucocorticoid treatment, with evidence of rapid hypermineralization and decreased lacunar size. Hypermineralization of the bone extracellular matrix likely contributed to the bone fragility that causes the collapse of osteonectroic subchondral bone and joint degredation (Fowler et al., 2017). PLR suppression is also apparent in osteoarthritis. Although previously thought to be a condition affecting primarily articular cartilage, a significant shift towards hypermineralization occurs in late-stage osteoarthritic bone, accompanying several other signs of PLR suppression. This observation suggests the important role of PLR in maintaining bone-cartilage crosstalk in healthy joints, and a mechanism by which PLR suppression in subchondral bone exacerbates joint disease (Mazur et al., 2019). Just as SRμCT data was pivotal in revealing the role of osteocytes in joint disease, this approach has potential to make clear mechanisms contributing to a variety of pathological musculoskeletal conditions.

6. Closing Remarks

Synchrotron radiation micro-computed tomography provides valuable information on the internal morphology, mineralization and crack path in bone. It does so through the reconstruction of high-quality image slices from scanned samples subjected to x-rays and is capable of resolving microscale-length features. This reconstructed data can be processed to quantify porosity size and density in bone as an indicator of bone quantity, as well as structural, mineral composition (vTMD), and osteocyte lacunar quantification as indicators of bone quality. These parameters are but a few of the wide variety of information that can potentially be supplied through the use of SRμCT (Table 1), and as synchrotron and lab-based CT techniques become more advanced, other mechanisms controlling bone quality are becoming more clear. Additionally, due to toughening mechanisms acting at every length-scale in the hierarchical structure of bone, examining features at the microscale assists in understanding the unique ability of bone to resist fracture and how this ability is degraded with disease. Because extrinsic toughening mechanisms such as crack deflection and twist occur predominantly at the microscale, SRμCT is appropriately used to visualize and quantify crack deflection around highly mineralized regions.

Application of SRμCT to assess bone quality and fracture mechanisms, particularly in unhealthy bone, is paramount for improving quality of life. No clear trends exist connecting bone fragility to lacunar size or density when studying PLR suppression through glucocorticoid-induced osteonecrosis, vitamin D deficiency, and cochlear bone with an MMP13 protease deficiency. This indicates that the factors responsible for controlling lacunar size and shape remain to be fully explored. Recent work in resistance to fracture does indicate that increased Haversian canal and osteonal density, in conjunction with larger and more frequent

microcracks, contribute to lower toughness in aged bone due to a higher number of hypermineralized cement lines present for crack propagation to occur.

The longitudinally oriented cement lines in human bone and the lamellae layers in murine bone have been found to be the main source of crack deflection. Comparisons between healthy and fragile bones reveal that osteonal organization and mineralization of bone matrix play a large role in bone quality as well. Hypermineralization found in conditions such as OI and a vitamin D deficiency is thought to increase bone fragility, and hypomineralization is thought to contribute to the plasticity of bone seen in PDB. These applications showcase the diversity of SRμCT and also display how research using SRμCT has advanced understanding of bone quality through study of microstructure, fracture mechanisms, and mineralization.

Declaration of competing interest

The authors have no conflicts of interest.

Credit Author Statement

Yoshihiro Obata: Writing - Original Draft, Writing - Review & Editing **Hrishikesh A. Bale:** Writing - Review & Editing **Harold S. Barnard:** Writing - Review & Editing **Dula Y. Parkinson:** Writing - Review & Editing **Tamara N. Alliston:** Writing - Review & Editing **Claire Acevedo:** Writing - Original Draft, Writing - Review & Editing

Acknowledgments

References

Claire Acevedo, Hrishikesh Bale, Bernd Gludovatz, Amy Wat, Simon Y. Tang, Mingyue Wang, Björn Busse, Elizabeth A. Zimmermann, Eric Schaible, Matthew R. Allen, David B. Burr, and Robert O. Ritchie. Alendronate treatment alters bone tissues at multiple structural levels in healthy canine cortical bone. *Bone*, 81:352–363, 2015. ISSN 87563282. doi: 10.1016/j.bone.2015.08.002. URL `http://dx.doi.org/10.1016/j.bone.2015.08.002`.

Claire Acevedo, Vincent A. Stadelmann, Dominique P. Pioletti, Tamara Alliston, and Robert O. Ritchie. Fatigue as the missing link between bone fragility and fracture. *Nature Biomedical Engineering*, 2(2):62–71, 2018a. ISSN 2157846X. doi: 10.1038/s41551-017-0183-9. URL `http://dx.doi.org/10.1038/s41551-017-0183-9`.

Claire Acevedo, Meghan Sylvia, Eric Schaible, James L. Graham, Kimber L. Stanhope, Lionel N. Metz, Bernd Gludovatz, Ann V. Schwartz, Robert O. Ritchie, Tamara N. Alliston, Peter J. Havel, and Aaron J. Fields. Contributions of Material Properties and Structure to Increased Bone Fragility for a Given Bone Mass in the UCD-T2DM Rat Model of Type 2 Diabetes. *Journal of Bone and Mineral Research*, 33(6): 1066–1075, 2018b. ISSN 15234681. doi: 10.1002/jbmr.3393.

III W. Ager, G. Balooch, and R. O. Ritchie. Fracture, aging, and disease in bone. *Journal of Materials Research*, 21(8):1878–1892, 2006. ISSN 08842914. doi: 10.1557/jmr.2006.0242.

Joanna Aizenberg, James C. Weaver, Monica S. Thanawala, Vikram C. Sundar, Daniel E. Morse, and Peter Fratzl. Materials science: Skeleton of euplectella sp.: Structural hierarchy from the nanoscale to the macroscale. *Science*, 309(5732):275–278, 2005. ISSN 00368075. doi: 10.1126/science.1112255.

Burcu Akça and Salih Z. Erzeneoğlu. The mass attenuation coefficients, electronic, atomic, and molecular cross sections, effective atomic numbers, and electron densities for compounds of some biomedically important elements at 59.5 kev. *Science and Technology of Nuclear Installations*, 2014, 2014. ISSN 16876083. doi: 10.1155/2014/901465.

Tamara Alliston. Biological regulation of bone quality. *Current Osteoporosis Reports*, 12(3):366–375, 2014. ISSN 15442241. doi: 10.1007/s11914-014-0213-4.

Harold S. Barnard, A. A. MacDowell, D. Y. Parkinson, P. Mandal, M. Czabaj, Y. Gao, E. Maillet, B. Blank, N. M. Larson, R. O. Ritchie, B. Gludovatz, C. Acevedo, and D. Liu. Synchrotron X-ray micro-tomography at the Advanced Light Source: Developments in high-temperature in-situ mechanical testing. *Journal of Physics: Conference Series*, 849(1), 2017. ISSN 17426596. doi: 10.1088/1742-6596/849/1/012043.

Holly D. Barth, Maximilien E. Launey, Alastair A. MacDowell, Joel W. Ager, and Robert O. Ritchie. On the effect of X-ray irradiation on the deformation and fracture behavior of human cortical bone. *Bone*, 46(6):1475–1485, 2010. ISSN 87563282. doi: 10.1016/j.bone.2010.02.025. URL http://dx.doi.org/10.1016/j.bone.2010.02.025.

Holly D. Barth, Elizabeth A. Zimmermann, Eric Schaible, Simon Y. Tang, Tamara Alliston, and Robert O. Ritchie. Characterization of the effects of x-ray irradiation on the hierarchical structure and mechanical properties of human cortical bone. *Biomaterials*, 32(34):8892–8904, 2011. ISSN 01429612. doi: 10.1016/j.biomaterials.2011.08.013.

S Bayat, L Apostol, E Boller, T Brochard, and F Peyrin. In vivo imaging of bone micro-architecture in mice with 3d synchrotron radiation micro-tomography. *Nuclear Instruments and Methods in Physics Research Section A: Accelerators, Spectrometers, Detectors and Associated Equipment*, 548(1-2):247–252, 2005.

Harun H. Bayraktar, Elise F. Morgan, Glen L. Niebur, Grayson E. Morris, Eric K. Wong, and Tony M. Keaveny. Comparison of the elastic and yield properties of human femoral trabecular and cortical bone tissue. *Journal of Biomechanics*, 37(1):27–35, 2004. ISSN 00219290. doi: 10.1016/S0021-9290(03)00257-4.

Teresita Bellido. Osteocyte-driven bone remodeling. *Calcified Tissue International*, 94(1):25–34, 2014. ISSN 0171967X. doi: 10.1007/s00223-013-9774-y.

Ricardo Bernhardt, Dieter Scharnweber, Bert Müller, P Thurner, H Schliephake, P Wyss, F Beckmann, Jürgen Goebbels, and H Worch. Comparison of microfocus-and synchrotron x-ray tomography for the analysis of osteointegration around ti6al4v implants. *Eur Cell Mater*, 7(42):e51, 2004.

Lynda F Bonewald. Mechanosensation and transduction in osteocytes. *BoneKEy osteovision*, 3(10):7, 2006.

Lynda F. Bonewald. Osteocytes as dynamic multifunctional cells. *Annals of the New York Academy of Sciences*, 1116:281–290, 2007. ISSN 17496632. doi: 10.1196/annals.1402.018.

Lynda F. Bonewald. The amazing osteocyte. *Journal of Bone and Mineral Research*, 26(2):229–238, 2011. ISSN 08840431. doi: 10.1002/jbmr.320.

Mary L Bouxsein, Stephen K Boyd, Blaine A Christiansen, Robert E Guldberg, Karl J Jepsen, and Ralph Müller. Guidelines for assessment of bone microstructure in rodents using micro–computed tomography. *Journal of bone and mineral research*, 25(7):1468–1486, 2010.

Helen R. Buie, Graeme M. Campbell, R. Joshua Klinck, Joshua A. MacNeil, and Steven K. Boyd. Automatic segmentation of cortical and trabecular compartments based on a dual threshold technique for in vivo micro-CT bone analysis. *Bone*, 41(4):505–515, 2007. ISSN 87563282. doi: 10.1016/j.bone.2007.07.007.

E. H. Burger and J. Klein-Nulend. Mechanotransduction in bone - Role of the lacuno-canalicular network. *FASEB Journal*, 13(8 SUPPL.):101–112, 1999. ISSN 08926638.

Andrew J. Burghardt, Yongmei Wang, Hashem Elalieh, Xavier Thibault, Daniel Bikle, Françoise Peyrin, and Sharmila Majumdar. Evaluation of fetal bone structure and mineralization in IGF-I deficient mice using synchrotron radiation microtomography and Fourier transform infrared spectroscopy. *Bone*, 40(1): 160–168, 2007. ISSN 87563282. doi: 10.1016/j.bone.2006.06.017.

D. B. Burr. The contribution of the organic matrix to bone's material properties. *Bone*, 31(1):8–11, 2002. ISSN 87563282. doi: 10.1016/S8756-3282(02)00815-3. URL `http://dx.doi.org/10.1016/S8756-3282(02)00815-3`.

David B. Burr. Bone quality: Understanding what matters. *Journal of Musculoskeletal Neuronal Interactions*, 4(2):184–186, 2004. ISSN 11087161.

Björn Busse, Hrishikesh A. Bale, Elizabeth A. Zimmermann, Brian Panganiban, Holly D. Barth, Alessandra Carriero, Eik Vettorazzi, Josef Zustin, Michael Hahn, Joel W. Ager, Klaus Püschel, Michael Amling, and Robert O. Ritchie. Vitamin D deficiency induces early signs of aging in human bone, increasing the risk of fracture. *Science Translational Medicine*, 5(193), 2013. ISSN 19466234. doi: 10.1126/scitranslmed.3006286.

Jorge Cano, Julián Campo, Juan José Vaquero, Jose María Martínez-González, Antonio Bascones, et al. High resolution image in bone biology ii. review of the literature. *Medicina Oral Patologia Oral y Cirugia Bucal*, 13(1):31, 2008.

Holly D Carlton, John W Elmer, Yan Li, Mario Pacheco, Deepak Goyal, Dilworth Y Parkinson, and Alastair A MacDowell. Using synchrotron radiation microtomography to investigate multi-scale three-dimensional microelectronic packages. *JoVE (Journal of Visualized Experiments)*, (110):e53683, 2016.

Alessandra Carriero, Elizabeth A. Zimmermann, Adriana Paluszny, Simon Y. Tang, Hrishikesh Bale, Bjorn Busse, Tamara Alliston, Galateia Kazakia, Robert O. Ritchie, and Sandra J. Shefelbine. How tough is brittle bone? Investigating osteogenesis imperfecta in mouse bone. *Journal of Bone and Mineral Research*, 29(6):1392–1401, 2014. ISSN 15234681. doi: 10.1002/jbmr.2172.

Yasmin Carter, C. David L. Thomas, John G. Clement, Andrew G. Peele, Kevin Hannah, and David M.L. Cooper. Variation in osteocyte lacunar morphology and density in the human femur - a synchrotron radiation micro-CT study. *Bone*, 52(1):126–132, 2013. ISSN 87563282. doi: 10.1016/j.bone.2012.09.010. URL `http://dx.doi.org/10.1016/j.bone.2012.09.010`.

R Cerbino, L Peverini, MAC Potenza, A Robert, P Bösecke, and M Giglio. X-ray-scattering information obtained from near-field speckle. *Nature Physics*, 4(3):238–243, 2008.

Chang Chieh Cheng, Yu Tai Ching, Pai Hung Ko, and Yeukuang Hwu. Correction of center of rotation and projection angle in synchrotron X-ray computed tomography. *Scientific Reports*, 8(1):1–9, 2018. ISSN 20452322. doi: 10.1038/s41598-018-28149-8. URL `http://dx.doi.org/10.1038/s41598-018-28149-8`.

D. M.L. Cooper, B. Erickson, A. G. Peele, K. Hannah, C. D.L. Thomas, and J. G. Clement. Visualization of 3D osteon morphology by synchrotron radiation micro-CT. *Journal of Anatomy*, 219(4):481–489, 2011. ISSN 00218782. doi: 10.1111/j.1469-7580.2011.01398.x.

O. Cornu, X. Banse, P. L. Docquier, S. Luyckx, and Ch Delloye. Effect of freeze-drying and gamma irradiation on the mechanical properties of human cancellous bone. *Journal of Orthopaedic Research*, 18(3):426–431, 2000. ISSN 07360266. doi: 10.1002/jor.1100180314.

John D. Currey. Hierarchies in biomineral structures. *Science*, 309(5732):253–254, 2005. ISSN 00368075. doi: 10.1126/science.1113954.

E Dall'Ara, D Barber, and M Viceconti. About the inevitable compromise between spatial resolution and accuracy of strain measurement for bone tissue: a 3d zero-strain study. *Journal of biomechanics*, 47(12): 2956–2963, 2014.

Yoni De Witte, Matthieu Boone, Jelle Vlassenbroeck, Manuel Dierick, and Luc Van Hoorebeke. Bronnikov-aided correction for x-ray computed tomography. *JOSA A*, 26(4):890–894, 2009.

Neha S. Dole, Courtney M. Mazur, Claire Acevedo, Justin P. Lopez, David A. Monteiro, Tristan W. Fowler, Bernd Gludovatz, Flynn Walsh, Jenna N. Regan, Sara Messina, Daniel S. Evans, Thomas F. Lang, Bin Zhang, Robert O. Ritchie, Khalid S. Mohammad, and Tamara Alliston. Osteocyte-Intrinsic TGF-β Signaling Regulates Bone Quality through Perilacunar/Canalicular Remodeling. *Cell Reports*, 21(9):2585–2596, 2017. ISSN 22111247. doi: 10.1016/j.celrep.2017.10.115. URL https://doi.org/10.1016/j.celrep.2017.10.115.

Neha S. Dole, Cristal S. Yee, Courtney M. Mazur, Claire Acevedo, and Tamara Alliston. Tgfβ regulation of perilacunar/canalicular remodeling is sexually dimorphic. *bioRxiv*, 2019. doi: 10.1101/737395. URL https://www.biorxiv.org/content/early/2019/08/16/737395.

Pei Dong, Sylvain Haupert, Bernhard Hesse, Max Langer, Pierre Jean Gouttenoire, Valérie Bousson, and Françoise Peyrin. 3D osteocyte lacunar morphometric properties and distributions in human femoral cortical bone using synchrotron radiation micro-CT images. *Bone*, 60:172–185, 2014. ISSN 87563282. doi: 10.1016/j.bone.2013.12.008. URL http://dx.doi.org/10.1016/j.bone.2013.12.008.

Eve Donnelly. Methods for assessing bone quality: A review. *Clinical Orthopaedics and Related Research*, 469(8):2128–2138, 2011. ISSN 15281132. doi: 10.1007/s11999-010-1702-0.

Anton du Plessis, Stephan Gerhard le Roux, and Anina Guelpa. The ct scanner facility at stellenbosch university: an open access x-ray computed tomography laboratory. *Nuclear Instruments and Methods in Physics Research Section B: Beam Interactions with Materials and Atoms*, 384:42–49, 2016.

Sarah K Easley, Michael G Jekir, Andrew J Burghardt, Mei Li, and Tony M Keaveny. Contribution of the intra-specimen variations in tissue mineralization to pth-and raloxifene-induced changes in stiffness of rat vertebrae. *Bone*, 46(4):1162–1169, 2010.

B. Ettinger, D. B. Burr, and R. O. Ritchie. Proposed pathogenesis for atypical femoral fractures: Lessons from materials research. *Bone*, 55(2):495–500, 2013. ISSN 87563282. doi: 10.1016/j.bone.2013.02.004. URL http://dx.doi.org/10.1016/j.bone.2013.02.004.

Dieter Felsenberg and Steven Boonen. The bone quality framework: Determinants of bone strength and their interrelationships, and implications for osteoporosis management. *Clinical Therapeutics*, 27(1):1–11, 2005. ISSN 1879114X. doi: 10.1016/j.clinthera.2004.12.020.

M Feser, J Gelb, H Chang, H Cui, F Duewer, SH Lau, A Tkachuk, and W Yun. Sub-micron resolution ct for failure analysis and process development. *Measurement science and technology*, 19(9):094001, 2008.

Tristan W. Fowler, Claire Acevedo, Courtney M. Mazur, Faith Hall-Glenn, Aaron J. Fields, Hrishikesh A. Bale, Robert O. Ritchie, Jeffrey C. Lotz, Thomas P. Vail, and Tamara Alliston. Glucocorticoid suppression of osteocyte perilacunar remodeling is associated with subchondral bone degeneration in osteonecrosis. *Scientific Reports*, 7(February):1–13, 2017. ISSN 20452322. doi: 10.1038/srep44618. URL http://dx.doi.org/10.1038/srep44618.

Peter Fratzl. Biomimetic materials research: What can we really learn from nature's structural materials? *Journal of the Royal Society Interface*, 4(15):637–642, 2007. ISSN 17425662. doi: 10.1098/rsif.2007.0218.

Peter Fratzl and Richard Weinkamer. Nature's hierarchical materials. *Progress in Materials Science*, 52(8):1263–1334, 2007.

Rémy Gauthier, Hélène Follet, Cécile Olivier, David Mitton, and Françoise Peyrin. 3D analysis of the osteonal and interstitial tissue in human radii cortical bone. *Bone*, 127(January):526–536, 2019. ISSN 87563282. doi: 10.1016/j.bone.2019.07.028. URL https://doi.org/10.1016/j.bone.2019.07.028.

Harry K Genant, Cyrus Cooper, Gyula Poor, Ian Reid, George Ehrlich, J Kanis, BE Christopher Nordin, Elizabeth Barrett-Connor, Dennis Black, J-P Bonjour, et al. Interim report and recommendations of the world health organization task-force for osteoporosis. *Osteoporosis International*, 10(4):259–264, 1999.

Maude Gerbaix, Vasily Gnyubkin, Delphine Farlay, Cécile Olivier, Patrick Ammann, Guillaume Courbon, Norbert Laroche, Rachel Genthial, Hélène Follet, Françoise Peyrin, Boris Shenkman, Guillemette Gauquelin-Koch, and Laurence Vico. One-month spaceflight compromises the bone microstructure, tissue-level mechanical properties, osteocyte survival and lacunae volume in mature mice skeletons. *Scientific reports*, 7(1):2659, 2017. ISSN 20452322. doi: 10.1038/s41598-017-03014-2.

F Gillard, Richard Boardman, Mark Mavrogordato, Dave Hollis, Ian Sinclair, Fabrice Pierron, and Martin Browne. The application of digital volume correlation (dvc) to study the microstructural behaviour of trabecular bone during compression. *Journal of the mechanical behavior of biomedical materials*, 29:480–499, 2014.

Ingo Grafe, Tao Yang, Stefanie Alexander, Erica P. Homan, Caressa Lietman, Ming Ming Jiang, Terry Bertin, Elda Munivez, Yuqing Chen, Brian Dawson, Yoshihiro Ishikawa, Mary Ann Weis, T. Kuber Sampath, Catherine Ambrose, David Eyre, Hans Peter Bächinger, and Brendan Lee. Excessive transforming growth factor-β 2 signaling is a common mechanism in osteogenesis imperfecta. *Nature Medicine*, 20(6):670–675, 2014. ISSN 1546170X. doi: 10.1038/nm.3544.

Doğa Gürsoy, Francesco De Carlo, Xianghui Xiao, and Chris Jacobsen. TomoPy: A framework for the analysis of synchrotron tomographic data. *Journal of Synchrotron Radiation*, 21(5):1188–1193, 2014. ISSN 16005775. doi: 10.1107/S1600577514013939.

Bernhard Hesse, Max Langer, Peter Varga, Alexandra Pacureanu, Pei Dong, Susanne Schrof, Nils Manünicke, Heikki Suhonen, Cecile Olivier, Peter Maurer, Galateia J. Kazakia, Kay Raum, and Francoise Peyrin. Alterations of mass density and 3D osteocyte lacunar properties in bisphosphonate-related osteonecrotic human jaw bone, a synchrotron μCT study. *PLoS ONE*, 9(2):1–11, 2014a. ISSN 19326203. doi: 10.1371/journal.pone.0088481.

Bernhard Hesse, Nils Maennicke, Alexandra Pacureanu, Peter Varga, Max Langer, Peter Maurer, Francoise Peyrin, and Kay Raum. Accessing osteocyte lacunar geometrical properties in human jaw bone on the submicron length scale using synchrotron radiation μct. *Journal of microscopy*, 255(3):158–168, 2014b.

Bernhard Hesse, Peter Varga, Max Langer, Alexandra Pacureanu, Susanne Schrof, Nils Männicke, Heikki Suhonen, Peter Maurer, Peter Cloetens, Francoise Peyrin, et al. Canalicular network morphology is the major determinant of the spatial distribution of mass density in human bone tissue: evidence by means of synchrotron radiation phase-contrast nano-ct. *Journal of bone and mineral research*, 30(2):346–356, 2015a.

Bernhard Hesse, Peter Varga, Max Langer, Alexandra Pacureanu, Susanne Schrof, Nils Männicke, Heikki Suhonen, Peter Maurer, Peter Cloetens, Francoise Peyrin, et al. Canalicular network morphology is the major determinant of the spatial distribution of mass density in human bone tissue: evidence by means of synchrotron radiation phase-contrast nano-ct. *Journal of bone and mineral research*, 30(2):346–356, 2015b.

Godfrey N Hounsfield. Computerized transverse axial scanning (tomography): Part 1. description of system. *The British journal of radiology*, 46(552):1016–1022, 1973.

Rik Huiskes, Ronald Rulmerman, G. Harry Van Lenthe, and Jan D. Janssen. Effects of mechanical forces on maintenance and adaptation of form in trabecular bone. *Nature*, 405(6787):704–706, 2000. ISSN 00280836. doi: 10.1038/35015116.

Jason A. Inzana, Jason R. Maher, Masahiko Takahata, Edward M. Schwarz, Andrew J. Berger, and Hani A. Awad. Bone fragility beyond strength and mineral density: Raman spectroscopy predicts femoral fracture toughness in a murine model of rheumatoid arthritis. *Journal of Biomechanics*, 46(4):723–730, 2013. ISSN 00219290. doi: 10.1016/j.jbiomech.2012.11.039. URL http://dx.doi.org/10.1016/j.jbiomech.2012.11.039.

Masako Ito. Assessment of bone quality using micro-computed tomography (micro-ct) and synchrotron micro-ct. *Journal of bone and mineral metabolism*, 23(1):115–121, 2005.

John R. Jameson, Carolyne I. Albert, Bjoern Busse, Peter A. Smith, and Gerald F. Harris. 3D micron-scale imaging of the cortical bone canal network in human osteogenesis imperfecta (OI). *Medical Imaging 2013: Biomedical Applications in Molecular, Structural, and Functional Imaging*, 8672(March 2013):86721L, 2013. ISSN 16057422. doi: 10.1117/12.2007209.

Emmanuel J. Jáuregui, Omar Akil, Claire Acevedo, Faith Hall-Glenn, Betty S. Tsai, Hrishikesh A. Bale, Ellen Liebenberg, Mary Beth Humphrey, Robert O. Ritchie, Lawrence R. Lustig, and Tamara Alliston. Parallel mechanisms suppress cochlear bone remodeling to protect hearing. *Bone*, 89:7–15, 2016. ISSN 87563282. doi: 10.1016/j.bone.2016.04.010. URL http://dx.doi.org/10.1016/j.bone.2016.04.010.

Avinash C Kak, Malcolm Slaney, and Ge Wang. Principles of computerized tomographic imaging. *Medical Physics*, 29(1):107–107, 2002a.

Avinash C Kak, Malcolm Slaney, and Ge Wang. Principles of computerized tomographic imaging. *Medical Physics*, 29(1):107–107, 2002b.

Jenneke Klein-Nulend, Aviral Vatsa, Rommel G. Bacabac, S. Djien Tan, and Theo H. Smit. The role of osteocytes in bone mechanotransduction. *Current Opinion in Orthopaedics*, 16(5):316–324, 2005. ISSN 10419918. doi: 10.1097/01.bco.0000177409.72833.ba.

K. J. Koester, J. W. Ager, and R. O. Ritchie. The true toughness of human cortical bone measured with realistically short cracks. *Nature Materials*, 7(8):672–677, 2008. ISSN 14764660. doi: 10.1038/nmat2221.

K. J. Koester, H. D. Barth, and R. O. Ritchie. Effect of aging on the transverse toughness of human cortical bone: Evaluation by R-curves. *Journal of the Mechanical Behavior of Biomedical Materials*, 4(7):1504–1513, 2011. ISSN 17516161. doi: 10.1016/j.jmbbm.2011.05.020. URL http://dx.doi.org/10.1016/j.jmbbm.2011.05.020.

H Labriet, C Nemoz, M Renier, P Berkvens, T Brochard, R Cassagne, Hélène Elleaume, François Estève, Camille Verry, Jacques Balosso, et al. Significant dose reduction using synchrotron radiation computed tomography: first clinical case and application to high resolution ct exams. *Scientific reports*, 8(1):1–7, 2018.

Nancy E. Lane and Wei Yao. Glucocorticoid-induced bone fragility: New insights. *Annals of the New York Academy of Sciences*, 1192:81–83, 2010. ISSN 17496632. doi: 10.1111/j.1749-6632.2009.05228.x.

Max Langer, Alexandra Pacureanu, Heikki Suhonen, Quentin Grimal, Peter Cloetens, and Françoise Peyrin. X-Ray Phase Nanotomography Resolves the 3D Human Bone Ultrastructure. *PLoS ONE*, 7(8):1–7, 2012a. ISSN 19326203. doi: 10.1371/journal.pone.0035691.

Max Langer, Alexandra Pacureanu, Heikki Suhonen, Quentin Grimal, Peter Cloetens, and Françoise Peyrin. X-ray phase nanotomography resolves the 3d human bone ultrastructure. *PloS one*, 7(8), 2012b.

Aymeric Larrue, Aline Rattner, Norbert Laroche, Laurence Vico, and Françoise Peyrin. Feasibility of microcrack detection in human trabecular bone images from 3D synchrotron microtomography. *Annual International Conference of the IEEE Engineering in Medicine and Biology - Proceedings*, pages 3918–3921, 2007. ISSN 05891019. doi: 10.1109/IEMBS.2007.4353190.

Aymeric Larrue, Aline Rattner, Zsolt Andrei Peter, Cécile Olivier, Norbert Laroche, Laurence Vico, and Françoise Peyrin. Synchrotron radiation micro-CT at the Micrometer scale for the analysis of the three-dimensional morphology of microcracks in human trabecular bone. *PLoS ONE*, 6(7), 2011. ISSN 19326203. doi: 10.1371/journal.pone.0021297.

M. E. Launey, P. Y. Chen, J. McKittrick, and R. O. Ritchie. Mechanistic aspects of the fracture toughness of elk antler bone. *Acta Biomaterialia*, 6(4):1505–1514, 2010a. ISSN 17427061. doi: 10.1016/j.actbio.2009.11.026. URL http://dx.doi.org/10.1016/j.actbio.2009.11.026.

Maximilien E. Launey and Robert O. Ritchie. On the fracture toughness of advanced materials. *Advanced Materials*, 21(20):2103–2110, 2009. ISSN 09359648. doi: 10.1002/adma.200803322.

Maximilien E. Launey, Markus J. Buehler, and Robert O. Ritchie. On the Mechanistic Origins of Toughness in Bone. *Annual Review of Materials Research*, 40(1):25–53, 2010b. ISSN 1531-7331. doi: 10.1146/annurev-matsci-070909-104427.

Sophie Le Cann, Erika Tudisco, Mikael J. Turunen, Alessandra Patera, Rajmund Mokso, Magnus Tägil, Ola Belfrage, Stephen A. Hall, and Hanna Isaksson. Investigating the mechanical characteristics of bone-metal implant interface using in situ synchrotron tomographic imaging. *Frontiers in Bioengineering and Biotechnology*, 6(JAN), 2019. ISSN 22964185. doi: 10.3389/fbioe.2018.00208.

Robert A Lewis. Medical phase contrast x-ray imaging: current status and future prospects. *Physics in medicine & biology*, 49(16):3573, 2004.

Yahui Liu, Jian Yao, Xiaohu Lu, Renping Xie, and Li Li. DeepCrack: A deep hierarchical feature learning architecture for crack segmentation. *Neurocomputing*, 338:139–153, 2019. ISSN 18728286. doi: 10.1016/j.neucom.2019.01.036.

Shaocheng Ma, Oliver Boughton, Angelo Karunaratne, Andi Jin, Justin Cobb, Ulrich Hansen, and Richard Abel. Synchrotron Imaging Assessment of Bone Quality. *Clinical Reviews in Bone and Mineral Metabolism*, 14(3):150–160, 2016. ISSN 15590119. doi: 10.1007/s12018-016-9223-3.

Alastair A. MacDowell, Harold Barnard, Dilworth Y. Parkinson, Abdel Haboub, Natalie Larson, Frank Zok, Francesco Parerai, Nagi N. Mansour, Hrishikesh Bale, Bernd Gludovatz, Claire Acevedo, Dong Liu, and Robert O. Ritchie. High temperature x-ray micro-tomography. *AIP Conference Proceedings*, 1741(July): 1–5, 2016. ISSN 15517616. doi: 10.1063/1.4952925.

Isabel S. Maggiano, Corey M. Maggiano, John G. Clement, C. David L. Thomas, Yasmin Carter, and David M.L. Cooper. Three-dimensional reconstruction of Haversian systems in human cortical bone using synchrotron radiation-based micro-CT: Morphology and quantification of branching and transverse connections across age. *Journal of Anatomy*, 228(5):719–732, 2016. ISSN 14697580. doi: 10.1111/joa.12430.

Sheridan C. Mayo, Andrew W. Stevenson, and Stephen W. Wilkins. In-Line Phase-Contrast X-ray Imaging and Tomography for Materials Science. *Materials*, 5(12):937–965, 2012. ISSN 1996-1944. doi: 10.3390/ma5050937.

Courtney M Mazur, Jonathon J Woo, Cristal S Yee, Aaron J Fields, Claire Acevedo, Karsyn N Bailey, Serra Kaya, Tristan W Fowler, Jeffrey C Lotz, Alexis Dang, et al. Osteocyte dysfunction promotes osteoarthritis through mmp13-dependent suppression of subchondral bone homeostasis. *Bone research*, 7(1):1–17, 2019.

Petar Milovanovic, Elizabeth A. Zimmermann, Michael Hahn, Danijela Djonic, Klaus Püschel, Marija Djuric, Michael Amling, and Björn Busse. Osteocytic canalicular networks: Morphological implications for altered mechanosensitivity. *ACS Nano*, 7(9):7542–7551, 2013a. ISSN 19360851. doi: 10.1021/nn401360u.

Petar Milovanovic, Elizabeth A. Zimmermann, Michael Hahn, Danijela Djonic, Klaus Püschel, Marija Djuric, Michael Amling, and Björn Busse. Osteocytic canalicular networks: Morphological implications for altered mechanosensitivity. *ACS Nano*, 7(9):7542–7551, 2013b. ISSN 19360851. doi: 10.1021/nn401360u.

Atsushi Momose, Shinya Kawamoto, Ichiro Koyama, Yoshitaka Hamaishi, Kengo Takai, and Yoshio Suzuki. Demonstration of x-ray talbot interferometry. *Japanese journal of applied physics*, 42(7B):L866, 2003.

Kaye S Morgan, David M Paganin, and Karen KW Siu. X-ray phase imaging with a paper analyzer. *Applied Physics Letters*, 100(12):124102, 2012.

Ralph Müller, H. Van Campenhout, B. Van Damme, G. Van Der Perre, J. Dequeker, T. Hildebrand, and P. Rüegsegger. Morphometric analysis of human bone biopsies: A quantitative structural comparison of histological sections and micro-computed tomography. *Bone*, 23(1):59–66, 1998. ISSN 87563282. doi: 10.1016/S8756-3282(98)00068-4.

Beat Münch, Pavel Trtik, Federica Marone, and Marco Stampanoni. Stripe and ring artifact removal with combined wavelet-Fourier filtering. *EMPA Activities*, 17(2009-2010 EMPA ACTIVITIES):34–35, 2009. ISSN 16601394. doi: 10.1364/oe.17.008567.
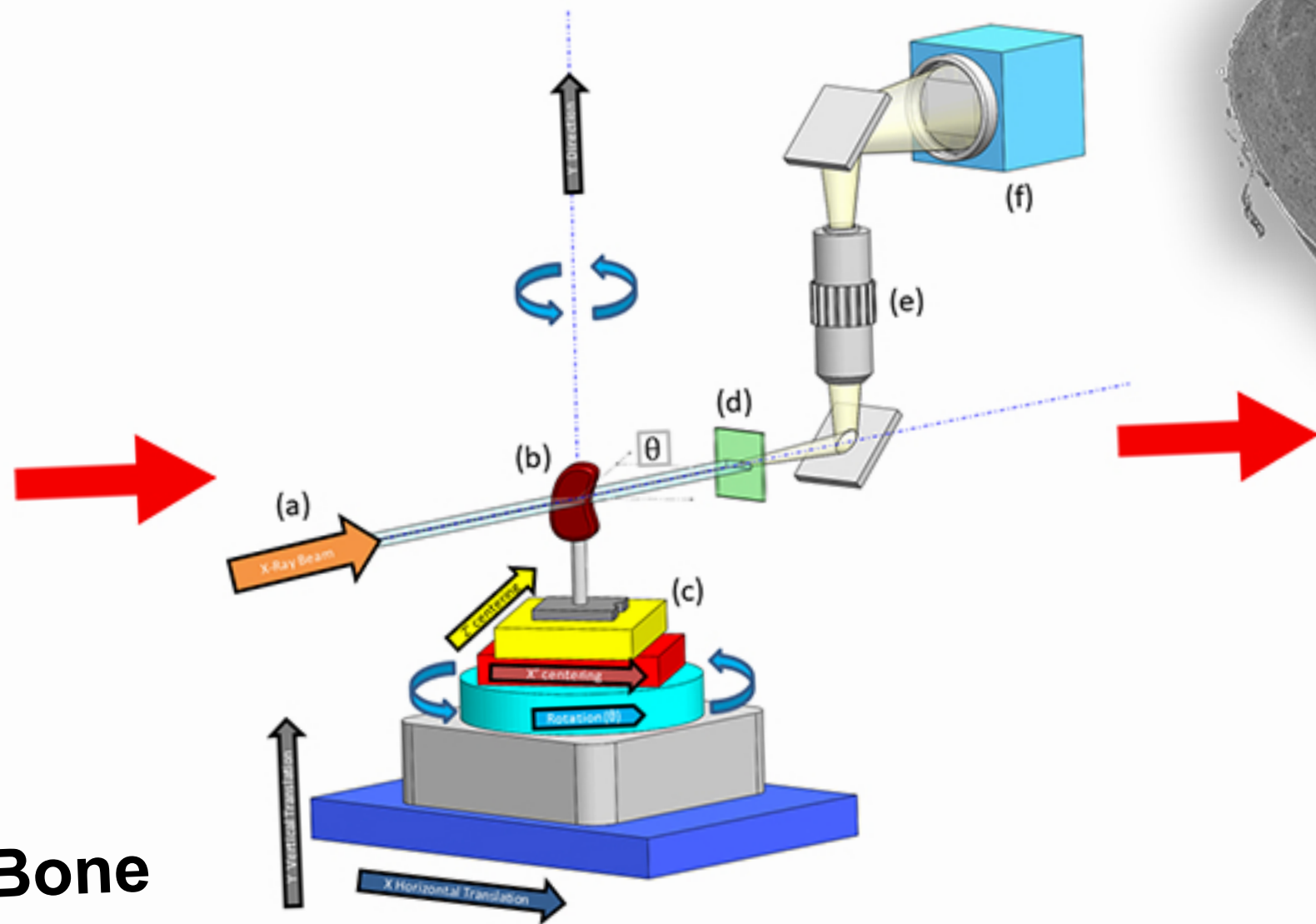
R. K. Nalla, J. H. Kinney, and R. O. Ritchie. Mechanistic fracture criteria for the failure of human cortical bone. *Nature Materials*, 2(3):164–168, 2003. ISSN 14761122. doi: 10.1038/nmat832.

R. K. Nalla, J. J. Kruzic, and R. O. Ritchie. On the origin of the toughness of mineralized tissue: Microcracking or crack bridging? *Bone*, 34(5):790–798, 2004. ISSN 87563282. doi: 10.1016/j.bone.2004.02.001.

R. K. Nalla, J. J. Kruzic, J. H. Kinney, and R. O. Ritchie. Mechanistic aspects of fracture and R-curve behavior in human cortical bone. *Biomaterials*, 26(2):217–231, 2005a. ISSN 01429612. doi: 10.1016/j.biomaterials.2004.02.017.

R. K. Nalla, J. S. Stölken, J. H. Kinney, and R. O. Ritchie. Fracture in human cortical bone: Local fracture criteria and toughening mechanisms. *Journal of Biomechanics*, 38(7):1517–1525, 2005b. ISSN 00219290. doi: 10.1016/j.jbiomech.2004.07.010.

Daniel P Nicolella, Donald E Moravits, Adrian M Gale, Lynda F Bonewald, and James Lankford. Osteocyte lacunae tissue strain in cortical bone. *Journal of biomechanics*, 39(9):1735–1743, 2006.

Sabah Nobakhti, Georges Limbert, and Philipp J. Thurner. Cement lines and interlamellar areas in compact bone as strain amplifiers - Contributors to elasticity, fracture toughness and mechanotransduction. *Journal of the Mechanical Behavior of Biomedical Materials*, 29:235–251, 2014. ISSN 17516161. doi: 10.1016/j.jmbbm.2013.09.011. URL http://dx.doi.org/10.1016/j.jmbbm.2013.09.011.

Shintaro Nomura and Teruko Takano-Yamamoto. Molecular events caused by mechanical stress in bone. *Matrix Biology*, 19(2):91–96, 2000. ISSN 0945053X. doi: 10.1016/S0945-053X(00)00050-0.

Juan A. Núñez, Alice Goring, Eric Hesse, Philipp J. Thurner, Philipp Schneider, and Claire E. Clarkin. Simultaneous visualisation of calcified bone microstructure and intracortical vasculature using synchrotron X-ray phase contrast-enhanced tomography. *Scientific Reports*, 7(1):1–9, 2017. ISSN 20452322. doi: 10.1038/s41598-017-13632-5.

Stefania Nuzzo, Françoise Peyrin, Peter Cloetens, José Baruchel, and Georges Boivin. Quantification of the degree of mineralization of bone in three dimensions using synchrotron radiation microtomography. *Medical Physics*, 29(11):2672–2681, 2002. ISSN 00942405. doi: 10.1118/1.1513161.

Jeffry S Nyman, Sasidhar Uppuganti, Alexander J Makowski, Barbara J Rowland, Alyssa R Merkel, Julie A Sterling, Todd L Bredbenner, and Daniel S Perrien. Predicting mouse vertebra strength with micro-computed tomography-derived finite element analysis. *BoneKEy reports*, 4, 2015.

Charles A. O'Brien, Dan Jia, Lilian I. Plotkin, Teresita Bellido, Cara C. Powers, Scott A. Stewart, Stavros C. Manolagas, and Robert S. Weinstein. Glucocorticoids act directly on osteoblasts and osteocytes to induce their apoptosis and reduce bone formation and strength. *Endocrinology*, 145(4):1835–1841, 2004. ISSN 00137227. doi: 10.1210/en.2003-0990.

Ramin Oftadeh, Miguel Perez-Viloria, Juan C. Villa-Camacho, Ashkan Vaziri, and Ara Nazarian. Biomechanics and Mechanobiology of Trabecular Bone: A Review. *Journal of Biomechanical Engineering*, 137 (1):1–15, 2015. ISSN 15288951. doi: 10.1115/1.4029176.

Alexandra Pacureanu, Max Langer, Elodie Boller, Paul Tafforeau, and Françoise Peyrin. Nanoscale imaging of the bone cell network with synchrotron x-ray tomography: optimization of acquisition setup. *Medical physics*, 39(4):2229–2238, 2012.

D. Paganin, S. C. Mayo, T. E. Gureyev, P. R. Miller, and S. W. Wilkins. Simultaneous phase and amplitude extraction from a single defocused image of a homogeneous object. *Journal of Microscopy*, 206(1):33–40, 2002. ISSN 00222720. doi: 10.1046/j.1365-2818.2002.01010.x.

M Palanca, AJ Bodey, M Giorgi, M Viceconti, D Lacroix, L Cristofolini, and E Dall'Ara. Synchrotron radiation for microtomography improves the precision of digital volume correlation for bone samples. In *Orthopaedic Proceedings*, volume 99, pages 29–29. The British Editorial Society of Bone & Joint Surgery, 2017.

Marco Palanca, Gianluca Tozzi, and Luca Cristofolini. The use of digital image correlation in the biomechanical area: a review. *International biomechanics*, 3(1):1–21, 2016.

Herwig Peterlik, Paul Roschger, Klaus Klaushofer, and Peter Fratzl. From brittle to ductile fracture of bone. *Nature Materials*, 5(1):52–55, 2006. ISSN 14764660. doi: 10.1038/nmat1545.

Terry Peters. CT Image Reconstruction. *Signal Processing Magazine, IEEE*, 14(1):67–74, 1997.

F Peyrin. Investigation of bone with synchrotron radiation imaging: from micro to nano. *Osteoporosis international*, 20(6):1057–1063, 2009.

Françoise Peyrin, Pei Dong, Alexandra Pacureanu, and Max Langer. Micro-and nano-ct for the study of bone ultrastructure. *Current osteoporosis reports*, 12(4):465–474, 2014a.

Françoise Peyrin, Pei Dong, Alexandra Pacureanu, and Max Langer. Micro-and nano-ct for the study of bone ultrastructure. *Current osteoporosis reports*, 12(4):465–474, 2014b.

Hai Qing and Lynda F. Bonewald. Osteocyte remodeling of the perilacunar and pericanalicular matrix. *International journal of oral science*, 1(2):59–65, 2009. ISSN 16742818. doi: 10.4248/ijos.09019.

Hai Qing, Laleh Ardeshirpour, Paola Divieti Pajevic, Vladimir Dusevich, Shigeaki Kato, John Wysolmerski, and Lynda F Bonewald. Remodeling in Mice during Lactation. *J Bone Miner Res*, 27(5):1018–1029, 2012. doi: 10.1002/jbmr.1567.Demonstration.

Carsten Raven. Numerical removal of ring artifacts in microtomography. *Review of Scientific Instruments*, 69(8):2978–2980, 1998. ISSN 00346748. doi: 10.1063/1.1149043.

Natalie Reznikov, Ron Shahar, and Steve Weiner. Bone hierarchical structure in three dimensions. *Acta Biomaterialia*, 10(9):3815–3826, 2014. ISSN 18787568. doi: 10.1016/j.actbio.2014.05.024. URL http://dx.doi.org/10.1016/j.actbio.2014.05.024.

Jae Young Rho, Liisa Kuhn-Spearing, and Peter Zioupos. Mechanical properties and the hierarchical structure of bone. *Medical Engineering and Physics*, 20(2):92–102, 1998. ISSN 13504533. doi: 10.1016/S1350-4533(98)00007-1.

R. O. Ritchie, R. K. Nalla, J. J. Kruzic, III W. Ager, G. Balooch, and J. H. Kinney. Fracture and ageing in bone: Toughness and structural characterization. *Strain*, 42(4):225–232, 2006. ISSN 00392103. doi: 10.1111/j.1475-1305.2006.00282.x.

Robert O Ritchie, Markus J Buehler, and Paul Hansma. Plasticity and toughness in bone. *Phys. Today*, 62 (6):41–47, 2009.

Andreas Roschger, P Roschger, Wolfgang Wagermaier, Junning Chen, AF van Tol, Felix Repp, S Blouin, A Berzlanovich, GM Gruber, K Klaushofer, et al. The contribution of the pericanalicular matrix to mineral content in human osteonal bone. *Bone*, 123:76–85, 2019.

Maite Ruiz-Yaniz, Irene Zanette, Adrian Sarapata, Lorenz Birnbacher, Mathias Marschner, Michael Chabior, Margie Olbinado, Franz Pfeiffer, and Alexander Rack. Hard x-ray phase-contrast tomography of non-homogeneous specimens: grating interferometry versus propagation-based imaging. *Journal of synchrotron radiation*, 23(5):1202–1209, 2016.

J Saban, MA Zussman, R Havey, AG Patwardhan, GB Schneider, and D King. Heterozygous oim mice exhibit a mild form of osteogenesis imperfecta. *Bone*, 19(6):575–579, 1996.

Murielle Salomé, Françoise Peyrin, Peter Cloetens, Christophe Odet, Anne Marie Laval-Jeantet, José Baruchel, and Per Spanne. A synchrotron radiation microtomography system for the analysis of trabecular bone samples. *Medical Physics*, 26(10):2194–2204, 1999. ISSN 00942405. doi: 10.1118/1.598736.

Steffen Schlüter, Adrian Sheppard, Kendra Brown, and Dorthe Wildenschild. Image processing of multiphase images obtained via X-ray microtomography: A review. *Water Resources Research*, 50(4):3615–3639, 2014. ISSN 19447973. doi: 10.1002/2014WR015256.

Felix N. Schmidt, Elizabeth A. Zimmermann, Flynn Walsh, Christine Plumeyer, Eric Schaible, Imke A.K. Fiedler, Petar Milovanovic, Manfred Rößle, Michael Amling, Clément Blanchet, Bernd Gludovatz, Robert O. Ritchie, and Björn Busse. On the Origins of Fracture Toughness in Advanced Teleosts: How the Swordfish Sword's Bone Structure and Composition Allow for Slashing under Water to Kill or Stun Prey. *Advanced Science*, 1900287, 2019. ISSN 21983844. doi: 10.1002/advs.201900287.

SCE Schuit, M Van der Klift, AEAM Weel, CEDH De Laet, H Burger, E Seeman, A Hofman, AG Uitterlinden, JPTM Van Leeuwen, and HAP Pols. Fracture incidence and association with bone mineral density in elderly men and women: the rotterdam study. *Bone*, 34(1):195–202, 2004.

Susanne Schweizer, Bodo Hattendorf, Philipp Schneider, Beat Aeschlimann, Ludwig Gauckler, Ralph Müller, and Detlef Günther. Preparation and characterization of calibration standards for bone density determination by micro-computed tomography. *Analyst*, 132(10):1040–1045, 2007.

Ego Seeman. Bone quality: The material and structural basis of bone strength. *Journal of Bone and Mineral Metabolism*, 26(1):1–8, 2008. ISSN 09148779. doi: 10.1007/s00774-007-0793-5.

DOetal Sillence, Alison Senn, and DM Danks. Genetic heterogeneity in osteogenesis imperfecta. *Journal of medical genetics*, 16(2):101–116, 1979.

P. E. Sinnett-Jones, M. Browne, W. Ludwig, J. Y. Buffière, and I. Sinclair. Microtomography assessment of failure in acrylic bone cement. *Biomaterials*, 26(33):6460–6466, 2005. ISSN 01429612. doi: 10.1016/j.biomaterials.2005.04.064.

Steven W. Smith. Special Imaging Techniques. *Digital Signal Processing*, pages 423–450, 2003. doi: 10.1016/b978-0-7506-7444-7/50062-5.

M Stampanoni, A Groso, A Isenegger, G Mikuljan, Q Chen, A Bertrand, S Henein, R Betemps, U Frommherz, P Böhler, et al. Trends in synchrotron-based tomographic imaging: the sls experience. *Developments in X-ray Tomography V*, 6318:63180M, 2006.

Henry Fox Talbot. Lxxvi. facts relating to optical science. no. iv. *The London, Edinburgh, and Dublin Philosophical Magazine and Journal of Science*, 9(56):401–407, 1836.

P. J. Thurner, P. Wyss, R. Voide, M. Stauber, M. Stampanoni, U. Sennhauser, and R. Müller. Time-lapsed investigation of three-dimensional failure and damage accumulation in trabecular bone using synchrotron light. *Bone*, 39(2):289–299, 2006. ISSN 87563282. doi: 10.1016/j.bone.2006.01.147.

Peter Varga, Alexandra Pacureanu, Max Langer, Heikki Suhonen, Bernhard Hesse, Quentin Grimal, Peter Cloetens, Kay Raum, and Françoise Peyrin. Investigation of the three-dimensional orientation of mineralized collagen fibrils in human lamellar bone using synchrotron x-ray phase nano-tomography. *Acta biomaterialia*, 9(9):8118–8127, 2013.

Peter Varga, Bernhard Hesse, Max Langer, Susanne Schrof, Nils Männicke, Heikki Suhonen, Alexandra Pacureanu, Dieter Pahr, Françoise Peyrin, and Kay Raum. Synchrotron x-ray phase nano-tomography-based analysis of the lacunar–canalicular network morphology and its relation to the strains experienced by osteocytes in situ as predicted by case-specific finite element analysis. *Biomechanics and modeling in mechanobiology*, 14(2):267–282, 2015.

F. P. Vidal, J. M. Létang, G. Peix, and P. Cloetens. Investigation of artefact sources in synchrotron microtomography via virtual X-ray imaging. *Nuclear Instruments and Methods in Physics Research, Section B: Beam Interactions with Materials and Atoms*, 234(3):333–348, 2005. ISSN 0168583X. doi: 10.1016/j.nimb.2005.02.003.

David W Wagner, Derek P Lindsey, and Gary S Beaupre. Deriving tissue density and elastic modulus from microct bone scans. *Bone*, 49(5):931–938, 2011.

Ji Wang, Galateia J Kazakia, Bin Zhou, X Tony Shi, and X Edward Guo. Distinct tissue mineral density in plate-and rod-like trabeculae of human trabecular bone. *Journal of Bone and Mineral Research*, 30(9): 1641–1650, 2015.

Ulrike G.K. Wegst, Hao Bai, Eduardo Saiz, Antoni P. Tomsia, and Robert O. Ritchie. Bioinspired structural materials. *Nature Materials*, 14(1):23–36, 2015. ISSN 14764660. doi: 10.1038/nmat4089.

Steve Weiner, Wolfie Traub, and H. Daniel Wagner. Lamellar bone: Structure-function relations. *Journal of Structural Biology*, 126(3):241–255, 1999. ISSN 10478477. doi: 10.1006/jsbi.1999.4107.

T Weitkamp, P Tafforeau, E Boller, P Cloetens, J-P Valade, P Bernard, F Peyrin, W Ludwig, L Helfen, and J Baruchel. Parallel-beam imaging at the esrf beamline id19: current status and plans for the future. In *AIP Conference Proceedings*, volume 1234, pages 83–86. American Institute of Physics, 2010.

P. J. Withers. Fracture mechanics by synchrotron X-ray microscopy. *Phil. Trans. R. Soc.*, A373:0157, 2015. doi: http://dx.doi.org/10.1098/rsta.2013.0157.

Ziling Wu, Ting Yang, Zhifei Deng, Baokun Huang, Han Liu, Yu Wang, Yuan Chen, Mary Caswell Stoddard, Ling Li, and Yunhui Zhu. Automatic Crack Detection and Analysis for Biological Cellular Materials in X-Ray In Situ Tomography Measurements. *Integrating Materials and Manufacturing Innovation*, 8(4):559–569, 2019. ISSN 21939772. doi: 10.1007/s40192-019-00162-3. URL https://doi.org/10.1007/s40192-019-00162-3.

Cristal S Yee, Charles A Schurman, Carter R White, and Tamara Alliston. Investigating osteocytic perilacunar/canalicular remodeling. *Current osteoporosis reports*, pages 1–12, 2019.

Yener N. Yeni and Timothy L. Norman. Calculation of porosity and osteonal cement line effects on the effective fracture toughness of cortical bone in longitudinal crack growth. *Journal of Biomedical Materials Research*, 51(3):504–509, 2000. ISSN 00219304. doi: 10.1002/1097-4636(20000905)51:3<504::AID-JBM27>3.0.CO;2-I.

Boliang Yu, Alexandra Pacureanu, Cécile Olivier, Peter Cloetens, and Françoise Peyrin. Assessment of the human bone lacuno-canalicular network at the nanoscale and impact of spatial resolution. *Scientific Reports*, 10(1):1–12, 2020.

Simon Zabler, Maximilian Ullherr, Christian Fella, Richard Schielein, Oliver Focke, Berit Zeller-Plumhoff, Pierre Lhuissier, Wesley DeBoever, and Randolf Hanke. Comparing image quality in phase contrast subμ x-ray tomography—a round-robin study. *Nuclear Instruments and Methods in Physics Research Section A: Accelerators, Spectrometers, Detectors and Associated Equipment*, 951:162992, 2020.

W. Zhang, S. S. Liao, and F. Z. Cui. Hierarchical self-assembly of nano-fibrils in mineralized collagen. *Chemistry of Materials*, 15(16):3221–3226, 2003. ISSN 08974756. doi: 10.1021/cm030080g.

Tunhe Zhou, Irene Zanette, Marie-Christine Zdora, Ulf Lundström, Daniel H Larsson, Hans M Hertz, Franz Pfeiffer, and Anna Burvall. Speckle-based x-ray phase-contrast imaging with a laboratory source and the scanning technique. *Optics letters*, 40(12):2822–2825, 2015.

Elizabeth A. Zimmermann and Robert O. Ritchie. Bone as a Structural Material. *Advanced Healthcare Materials*, 4(9):1287–1304, 2015. ISSN 21922659. doi: 10.1002/adhm.201500070.

Elizabeth A. Zimmermann, Maximilien E. Launey, Holly D. Barth, and Robert O. Ritchie. Mixed-mode fracture of human cortical bone. *Biomaterials*, 30(29):5877–5884, 2009. ISSN 01429612. doi: 10.1016/j.biomaterials.2009.06.017. URL http://dx.doi.org/10.1016/j.biomaterials.2009.06.017.

Elizabeth A. Zimmermann, Eric Schaible, Hrishikesh Bale, Holly D. Barth, Simon Y. Tang, Peter Reichert, Bjoern Busse, Tamara Alliston, Joel W. Ager, and Robert O. Ritchie. Erratum: Age-related changes in the plasticity and toughness of human cortical bone at multiple length scales (Proceedings of the National Academy of Sciences USA (2011) 108, 35 (14416-14421) DOI: 10.1073/pnas.1107966108). *Proceedings of the National Academy of Sciences of the United States of America*, 109(29):11890, 2012. ISSN 10916490. doi: 10.1073/pnas.1209596109.

Elizabeth A Zimmermann, Björn Busse, and Robert O Ritchie. The fracture mechanics of human bone: influence of disease and treatment. *BoneKEy Reports*, 4(June):1–13, 2015a. ISSN 20476396. doi: 10.1038/bonekey.2015.112.

Elizabeth A. Zimmermann, Till Köhne, Hrishikesh A. Bale, Brian Panganiban, Bernd Gludovatz, Joszef Zustin, Michael Hahn, Michael Amling, Robert O. Ritchie, and Björn Busse. Modifications to nano- and microstructural quality and the effects on mechanical integrity in Paget's disease of bone. *Journal of Bone and Mineral Research*, 30(2):264–273, 2015b. ISSN 15234681. doi: 10.1002/jbmr.2340.

Elizabeth A. Zimmermann, Eric Schaible, Bernd Gludovatz, Felix N. Schmidt, Christoph Riedel, Matthias Krause, Eik Vettorazzi, Claire Acevedo, Michael Hahn, Klaus Puschel, Simon Tang, Michael Amling, Robert O. Ritchie, and Bjorn Busse. Intrinsic mechanical behavior of femoral cortical bone in young, osteoporotic and bisphosphonate-treated individuals in low-and high energy fracture conditions. *Scientific Reports*, 6(January):1–12, 2016. ISSN 20452322. doi: 10.1038/srep21072. URL `http://dx.doi.org/10.1038/srep21072`.

Elizabeth A. Zimmermann, Christoph Riedel, Felix N. Schmidt, Kilian E. Stockhausen, Yuriy Chushkin, Eric Schaible, Bernd Gludovatz, Eik Vettorazzi, Federico Zontone, Klaus Püschel, Michael Amling, Robert O. Ritchie, and Björn Busse. Mechanical Competence and Bone Quality Develop During Skeletal Growth. *Journal of Bone and Mineral Research*, 00(0):1–12, 2019. ISSN 15234681. doi: 10.1002/jbmr.3730.

Qin Zou, Zheng Zhang, Qingquan Li, Xianbiao Qi, Qian Wang, and Song Wang. DeepCrack: Learning hierarchical convolutional features for crack detection. *IEEE Transactions on Image Processing*, 28(3):1498–1512, 2019. ISSN 10577149. doi: 10.1109/TIP.2018.2878966.

Cortical Bone

Synchrotron X-ray Micro-tomography

Microstructural Features

Mineralization

Crack Propagation

200 μm